Manuscript prepared for Atmos. Chem. Phys.
with version 2015/09/17 7.94 Copernicus papers of the LaTeX class copernicus.cls.
Date: 24 February 2016

Quantification of black carbon mixing state from traffic: implications for aerosol optical properties

M. D. Willis[1], R. M. Healy[2,3,a], N. Riemer[4], M. West[5], J. M. Wang[2], C.-H. Jeong[2], J. C. Wenger[3], G. J. Evans[2], J. P. D. Abbatt[1], and A. K. Y. Lee[1]

[1]Department of Chemistry, University of Toronto, Ontario, Canada
[2]Southern Ontario Centre for Atmospheric Aerosol Research, Department of Chemical Engineering and Applied Chemistry, University of Toronto, Ontario, Canada
[3]Department of Chemistry and Environmental Research Institute, University College Cork, Ireland
[4]Department of Atmospheric Sciences, University of Illinois at Urbana-Champaign, Urbana, USA
[5]Department of Mechanical Science and Engineering, University of Illinois at Urbana-Champaign, Urbana, USA
[a]Now at Air Monitoring and Transboundary Air Sciences Section, Environmental Monitoring and Reporting Branch, Ontario Ministry of the Environment and Climate Change, Ontario, Canada

Correspondence to: M.D. Willis (megan.willis@mail.utoronto.ca) and A.K.Y. Lee (alexky.lee@utoronto.ca)

Abstract. The climatic impacts of black carbon (BC) aerosol, an important absorber of solar radiation in the atmosphere, remain poorly constrained and are intimately related to its particle-scale physical and chemical properties. Using particle-resolved modelling informed by quantitative measurements from a soot-particle aerosol mass spectrometer, we confirm that the mixing state (the distribution of co-emitted aerosol amongst fresh BC-containing particles) at the time of emission significantly affects BC-aerosol optical properties even after a day of atmospheric processing. Both single particle and ensemble aerosol mass spectrometry observations indicate that BC near the point of emission co-exists with hydrocarbon-like organic aerosol (HOA) in two distinct particle types: HOA-rich and BC-rich particles. The average mass fraction of black carbon in HOA-rich and BC-rich ~~particles was 0.02 – 0.08 and 0.72 – 0.93~~particle classes was <0.1 and 0.8, respectively. Notably, approximately 90 % of BC mass resides in BC-rich particles. This new measurement capability provides quantitative insight into the physical and chemical nature of BC-containing particles and is used to drive a particle-resolved aerosol box model. Significant differences in calculated single scattering albedo (an increase of 0.1) arise from accurate treatment of initial particle mixing state as compared to the assumption of uniform aerosol composition at the point of BC injection into the atmosphere.

1 Introduction

Incomplete combustion emits teragram quantities of black carbon (BC) aerosol to the troposphere each year, resulting in a significant warming effect on climate that may be second only to carbon

dioxide (Bond et al., 2013; Ramanathan and Carmichael, 2008; Jacobson, 2001). BC influences climate directly, by absorbing solar radiation, and indirectly, by changing cloud properties and altering snow and ice melt. BC impacts on the global scale remain poorly constrained and are intimately related to its particle-scale physical and chemical properties (Bond et al., 2013). The majority of BC emissions in North America, Europe and Latin America are derived from traffic-related sources, though the specific physical and chemical properties of BC-containing particles at emission depend greatly on the source (Bond et al., 2013). BC-containing particles are generally hydrophobic near emission and become mixed over time with hydrophilic species through condensation and coagulation (Johnson et al., 2005; Moteki et al., 2007; Moffet and Prather, 2009), with resulting impacts on particle hygroscopicity (McMeeking et al., 2011b; Liu et al., 2013a; Laborde et al., 2013) and optical properties (Zhang et al., 2008; Cappa et al., 2012; Lack et al., 2012; Knox et al., 2009; Liu et al., 2015). Despite extensive previous work, our understanding of the role of mixing state in influencing the climate impacts of BC remains incomplete, in part because of instrumental challenges in particle characterization.

Studies assessing both the composition and amount of non-BC species in BC-containing particles are rare. A large body of evidence from urban, tunnel and engine emission studies has shown that individual combustion particles are mixtures of BC, inorganic species, metals, and hydrocarbon-like organic species at the time of emission (e.g., Johnson et al., 2005; Toner et al., 2006; Schneider et al., 2006; Tritscher et al., 2011; Chirico et al., 2010; Massoli et al., 2012; Zhang et al., 2013; Dallmann et al., 2014). Among these studies, single particle mass spectrometry has directly demonstrated mixing of BC and non-BC species in traffic-derived particles. For example, Toner et al. 2006 observed that emissions from heavy duty diesel engines were dominated by particles containing BC, organic species, calcium and phosphate, with one particle type dominated by BC and another with higher levels of organic species. In contrast, Healy et al. 2012 observed BC-dominated particles from traffic emissions in a European city. Other approaches to measure BC mixing state, including hygroscopicity and volatility differential mobility techniques, have highlighted the presence of an external mixture in terms of particle volatility with lower volatility, BC-containing aerosol being less hygroscopic (Kuwata et al., 2009; McMeeking et al., 2011a). Further, single particle soot photometer measurements of coating thickness in urban areas have shown that traffic-related BC-containing particles are largely uncoated or very thinly coated (Shiraiwa et al., 2008; McMeeking et al., 2011b; Laborde et al., 2013; Liu et al., 2014). In addition, microscopy studies have illustrated the dominance of bare or thinly coated BC-containing particles in traffic emissions (China et al., 2014) and the occurrence of coating, embedding and compaction of BC as it is aged (Adachi and Buseck, 2013; Adachi et al., 2014). While previous work has provided valuable insight into BC mixing state, the majority of past approaches have not allowed simultaneous quantification of BC mixing state on a mass basis and chemical characterization of non-BC species.

Considerable attention has been paid to BC-containing aerosol because of the potential for short-term climate mitigation through emissions reduction (Shindell et al., 2012). Therefore, a quantitative understanding of BC mixing state is crucial for three reasons: first, to assess rates of BC processing and removal in the atmosphere; second, to assess the role that BC-containing particles play as cloud nuclei; and third, to assess direct effects on solar radiation. Aerosol optical properties are central parameters required to evaluate direct radiative forcing (DRF). One of the largest contributors to uncertainty in DRF calculations is the single scattering albedo (SSA) (McComiskey et al., 2008), defined as the ratio of aerosol scattering to total light extinction. Previous work has clearly demonstrated that calculations of aerosol optical properties depend upon assumptions about particle mixing state (e.g., Jacobson, 2000), with assumptions of uniform internal mixing producing ~~overestimations in~~ overestimates of absorption efficiency and underestimates of single scattering albedo (Oshima et al., 2009; Zaveri et al., 2010; Matsui et al., 2013). The role of BC-aerosol mixing state at emission in affecting its mixing state in the atmosphere has also been highlighted in modelling studies explicitly treating detailed aerosol micro-physical and chemical processes (e.g., Matsui et al., 2013). However, model assessments driven by quantitative measurements of aerosol mixing state remain rare.

In this work, we use a soot-particle aerosol mass spectrometer, equipped with a light-scattering module, to determine the mixing state of BC-containing particles from traffic-dominated sources in an urban environment. These measurements provide quantitative insight into the physical and chemical nature of BC-containing particles near emission, and are used to drive a particle-resolved aerosol box model to assess the effect of accurately representing BC mixing on aerosol optical properties.

2 Methods

2.1 The soot-particle aerosol mass spectrometer (SP-AMS~~Measurements~~)

2.1.1 Two urban studies: locations and SP-AMS configuration

A soot-particle aerosol mass spectrometer (SP-AMS, Aerodyne Research Inc., Billerica, MA, USA), equipped with a light scattering module, was deployed in two urban studies to assess the mixing state of ~~rBC-containing~~ refractory black carbon (rBC) containing particles derived from vehicle emissions (Lee et al., 2015a). The first study was conducted in downtown Toronto away from major roadways (referred to as the "non-roadside" study), and the second was performed at ground level, near a busy road in downtown Toronto (referred to as the "roadside" study), to investigate fresh vehicle emissions. The ~~SP-AMS was operated such that both rBC-containing particles and non-rBC-containing particles were detected in the~~ non-roadside ~~study (see SI section 2), whereas exclusively rBC-containing particles were detected in the roadside study (Lee et al., 2015a; Onasch et al., 2012).~~

The non-roadside site is described in detail in Lee et al 2015a. The roadside study took place from May 31 to June 24, 2013 at the Southern Ontario Centre for Atmospheric Aerosol Research (SOCAAR) facility in downtown Toronto, Canada, located at ground level and adjacent to a road with traffic volumes ranging from 16000 to 25000 vehicles per day (Sabaliauskas et al., 2014). Ambient air was sampled at 170 $\mathrm{L\,min^{-1}}$ through a 10 cm (inner diameter) stainless steel tube fitted with a 2.5 $\mu\mathrm{m}$ cut-off inlet, located 15 m from the roadside at a height of 3 m above ground level a.g.l.

Two main modes of operation are possible with the SP-AMS, depending on the vaporizer configuration. The instrument was operated such that both rBC-containing particles and non-rBC-containing particles were detected in the non-roadside study (i.e., a dual-vaporizer configuration), whereas exclusively rBC-containing particles were detected in the roadside study (i.e., a laser-only configuration) (Lee et al., 2015a; Onasch et al., 2012).

2.1.2 SP-AMS operation and calibration

Details of the SP-AMS (and SP-AMS with light scattering) have been described elsewhere (Lee et al., 2015a; Onasch et al., 2012). The SP-AMS detects black carbon, which evaporates at ~4000 K, as C_x^+ fragments (predominantly m/z 12, 24, 36, 48 and 60) and is referred to as refractory black carbon (rBC) (Onasch et al., 2012). We use the term "black carbon" (BC) when referring generally to the concept of "soot"-type aerosol, while rBC is used when referring to quantities measured by the SP-AMS. In the SP-AMS, rBC and associated species are volatilized in an infrared laser beam (1064 nm) and are ionized using 70 eV electron impact ionization followed by detection in a time-of-flight mass spectrometer (ToF-MS) operated in "V-mode." For the majority of the study the SP-AMS was operated at one-minute time resolution alternating between bulk mass spectrum (MS), particle time-of-flight (pToF) and single particle modes. The SP-AMS was operated at high-time resolution (1 Hz) in MS mode for a total of five days during the roadside study. SP-AMS data was analysed using the Igor Pro-based analysis tool PIKA (Seuper, 2010). The single particle categorization procedure and k-means clustering algorithm k-means clustering algorithm that were used to analyse the single particle data followed the description in Lee et al. (2015a). Positive matrix factorization (PMF) analysis of ensemble data was performed to identify the sources of rBC and organics, and to speciate different types of organic species (i.e., oxygenated organic aerosol (OOA), biomass burning organic aerosol (BBOA), and hydrocarbon-like organic aerosol (HOA)), based on procedures described previously (Paatero and Tapper, 1994; Zhang et al., 2011; Ulbrich et al., 2009).

Without the tungsten vaporizer, direct calibrations of the ionization efficiency for $\mathrm{NH_4NO_3}$ ($\mathrm{IE_{NO_3}}$) are not possible. Therefore, size-selected (300 nm) Regal Black (Regal 400R Pigment, Cabot Corp.) particles were used to determine the mass based ionization efficiency of rBC ($\mathrm{mIE_{rBC}}$) (Onasch et al., 2012; Willis et al., 2014). The relative ionization efficiency for rBC ($\mathrm{RIE_{rBC}} = \mathrm{mIE_{rBC}}/\mathrm{mIE_{NO_3}}$) was 0.2 ± 0.05, as experimentally determined before removal of the tungsten vaporizer. Assuming that $\mathrm{RIE_{rBC}}$ is constant, $\mathrm{IE_{NO_3}}$ could be calculated based on known values of $\mathrm{mIE_{rBC}}$ and $\mathrm{RIE_{rBC}}$. The

average mIE_{rBC} was 189 ± 20 ions pg^{-1} in the roadside study. The calculated IE_{NO_3} was then used with recommended relative ionization efficiencies to quantify other aerosol species associated with rBC (Jimenez et al., 2003). Collection efficiency for rBC particles was determined in the roadside study using beam width probe (BWP) measurements described in (Willis et al., 2014). Ambient rBC-containing particles had an average beam width $\sigma = 0.46 \pm 0.03$ mm, which is close to, but wider than that of 300 nm Regal Black particles ($\sigma = 0.40 \pm 0.08$) (Willis et al., 2014). Therefore, a collection efficiency (CE) of 0.6 was applied for absolute quantification of rBC and associated species. A time-varying collection efficiency was not possible with BWP measurements available here; the assumption of a constant CE over periods of local and long-range transport influence in this study provided a good linear correlation with photoacoustic soot spectrometer (PASS) absorption measurements (405 and 781 nm) and SP-AMS rBC (Healy et al., 2015, Fig. 4). Note that the CE applied will not impact calculations of the mass fraction of rBC (mf_{rBC}). However, two additional uncertainties in SP-AMS measurements may affect calculation of mf_{rBC}. First, there are uncertainties in the recommended RIE for organic species evaporating from rBC in the SP-AMS of up to ~ 50 % (Lee et al., 2015a; Willis et al., 2014), which could cause an overestimation in the mass of coating material and a corresponding underestimation in mf_{rBC}. Second, it is possible for rBC-containing particles to pass through the edges of the laser vaporizer, thus producing a heating effect sufficient to evaporate some fraction of the coating materials but not evaporate the rBC itself. This effect may also lead to an underestimation in mf_{rBC}.SP-AMS CE and quantification are discussed in further detail in Supplement Sect. 1.

2.2 ~~Particle-resolved Box Model~~Photoacoustic soot spectrometer (PASS)

A photoacoustic soot spectrometer (PASS-3, Droplet Measurement Techniques, Boulder, CO) was used to measure aerosol absorption (b_{abs}) and scattering (b_{abs}) coefficients ($M\,m^{-1}$) at 405 and 781 nm. A 532 nm laser is not installed in this particular unit. The PASS determines aerosol absorption ($M\,m^{-1}$) in a cavity which acts as an acoustic resonator. The absorption of incoming radiation heats the particles, which in turn heat the surrounding air in the cavity (Arnott et al., 1999). The aerosol-laden air thus expands, resulting in a pressure disturbance. By modulating the laser power at the resonance frequency of the cavity, the pressure disturbance is amplified and the resulting acoustic wave is measured using a microphone. Light scattering at both wavelengths is concurrently measured using reciprocal nephelometry (Moosmüller et al., 2009; Flowers et al., 2010; Chan et al., 2011). Signals were not corrected for truncation; however, total particulate loading is relatively low at this site and saturation was not observed in scattering signals. Since a 532 nm laser was not present in this unit an NO_2 calibration was not possible, and the instrument was calibrated using a propane soot generator (miniCAST, 6203A, Jing). PASS measurements of the bulk single scattering albedo at 405 nm (selected due to superior signal-to-noise ratio for scattering relative to the 781 nm channel) are used here only to illustrate differences in optical properties in vehicle plumes with varying composition.

2.3 Particle-resolved box model simulations

We used the stochastic particle-resolved box model PartMC-MOSAIC (Particle Monte Carlo - Model for Simulating Aerosol Interactions and Chemistry) (Riemer et al., 2009; Zaveri et al., 2008) to quantify the importance of the observed mixing state information for the calculation of CCN and aerosol optical properties. PartMC-MOSAIC is suited for this task, as it explicitly tracks the composition of individual aerosol particles (in our case about 10^5 particles) in a population of different particle types within a well-mixed computational volume. Particle emissions, dilution with the background, and Brownian coagulation are simulated stochastically with PartMC, by generating a realization of a Poisson process using weighted particles in the sense of DeVille et al. (DeVille et al., 2011) and an accelerated binned sampling strategy (Michelotti et al., 2013). Coupled to PartMC is the MOSAIC chemistry code, which simulates gas chemistry (Zaveri and Peters, 1999), particle phase thermodynamics (Zaveri et al., 2005a, b), and dynamic gas-particle mass transfer (Zaveri et al., 2008) in a deterministic manner. ~~An important update to previous work is the sampling algorithm to assign the composition of individual particles of initial condition and particle emissions .~~

Here we compare two simulations that differ in the way the mixing state of the aerosol initial conditions and the aerosol emissions are prescribed. The set-up of the particle-resolved simulations is similar to the urban plume scenarios in Riemer et al. (2009) and Zaveri et al. (2010). Common to both simulations are the following specifics: The number of computational particles used in the simulation is about 10^5. The total simulation time is 24 h, with a simulation start of 06:00 local standard time (LST). The initial gas phase concentrations are the same as in Zaveri et al. (2010). In contrast to Zaveri et al. (2010), we prescribe a constant mixing height (400 m), relative humidity (70 $\%$) and temperature (298.15 K) to simplify the interpretation of the results. Since the entrainment of background aerosol can modify the aerosol mixing state substantially (Liu et al., 2011), we include constant dilution with the background at a rate of $1.5 \times 10^{-5}\ \mathrm{s}^{-1}$. The background aerosol is non-absorbing and consists of ammonium sulfate mixed with biogenic secondary organic aerosol. This dilution rate corresponds to about 75 $\%$ of the aerosol being replaced in a 24 h period, comparable to a diurnal mixing height increase of 500 m to 2000 m (e.g., Liu et al., 2011), although imposed uniformly over the day for simplicity. We also reduced the gas phase emissions by a factor of two compared to Zaveri et al. (2010) to create more moderately polluted conditions. The initial aerosol population was sampled from log-normal size distributions fitted from the measurement data, as shown in Table S1 in the Supplement. The derivation of model inputs from measurement data is described in Supplement Sect. 3.

To fully exploit the information supplied by the observations, we introduced a new method of sampling the aerosol composition for the aerosol initial conditions and emissions. We now allow for stochastic composition variation at each diameter, with a prescribed standard deviation around a mean value. ~~These parameters are quantitatively derived from measurements as described in Section 6 of the SI.~~ The new composition-sampling method proceeds as follows. For each aerosol particle,

the diameter is first sampled, and then the composition is sampled as a vector of mass fractions $\mathbf{w} = [w_{\mathrm{BC}}, w_{\mathrm{HOA}}]^\top$. Although we only sample two species for the simulations in this paper, we specify the sampling algorithm for any number of species. We use bold symbols to denote vectors, so $\mathbf{mf}$ is the mean mass fraction vector from Table S1 in the Supplement. We write Σ for the diagonal covariance matrix with diagonal entries $(\sigma_i)^2$, $\mathbf{1}$ for the vector of ones, and $\mathbf{x}^\top$ for the transpose of a vector $\mathbf{x}$. We sample the composition vector $\mathbf{w}$ from a multivariate normal distribution on the affine hyperplane of vectors that sum to one, truncated to the positive closed orthant (and thus to the probability or standard simplex). This is done as shown in Algorithm 1 using an accept-reject procedure.

~~The set-up of the simulations was similar to the urban plume scenarios presented in Riemer et al. (2009) and Zaveri et al. (2010). We tracked the evolution of gas phase species~~

Algorithm 1 Composition sampling

1: **repeat**
2: $\quad \mathbf{x} \leftarrow \mathcal{N}(\mathbf{mf}, \Sigma)$
3: $\quad \mathbf{w} \leftarrow \mathbf{x} + (1 - \mathbf{1}^\top \mathbf{x})\mathbf{mf}$
4: **until** $w_i \geq 0$ for all i

Algorithm 1 has five important properties, as follows. (1) It is clear that if the algorithm terminates then $\mathbf{w}$ lies in the positive closed orthant, so every species has a non-negative mass fraction. (2) The sum of the sampled mass fractions $\mathbf{w}$ is one, as can be seen from $\mathbf{1}^\top \mathbf{w} = \mathbf{1}^\top \mathbf{x} + (1 - \mathbf{1}^\top \mathbf{x})\mathbf{1}^\top \mathbf{mf} = \mathbf{1}^\top \mathbf{x} + 1 - \mathbf{1}^\top \mathbf{x} = 1$, assuming that the mean mass fractions sum to one and so $\mathbf{1}^\top \mathbf{mf} = 1$. (3) The distribution of $\mathbf{w}$ is a truncated multivariate normal, which follows from the fact that $\mathbf{x}$ has a multivariate normal distribution, $\mathbf{w}$ is an affine function of $\mathbf{x}$, and the accept-reject procedure samples from the truncation of the per-iteration distribution. Note, however, that the resulting marginal distributions for each single-species mass fraction will not in general have mean and standard deviation given by mf_i and ~~aerosol particles in a Lagrangian air parcel that was advected over and beyond a large urban area. The simulation started at 06:00 local standard time (LST) and , during the advection process, primary trace gases and aerosol particles from traffic sources were emitted into the air parcel for 12 . After 18:00 LST,~~ σ_i, respectively. (4) Adding additional species with zero mean mass fraction and zero standard deviation will not change the distribution of the other sampled mass fractions, as the additional species will have zero components in both $\mathbf{x}$ and $\mathbf{w}$ and will not alter the calculation of any other components. (5) Finally, the algorithm will terminate with probability one, under the conditions that that the mean mass fractions sum to one and each σ_i is non-negative and zero only if the corresponding mf_i is non-negative. This last property can be seen by first considering the set A of $\mathbf{x}$ that will result in a $\mathbf{w}$ in the positive closed orthant, terminating the algorithm. This set A is exactly the direct sum of the probability simplex with the span of $\{\mathbf{mf}\}$, as can be seen by checking that $\mathbf{x} = \mathbf{p} + \alpha\mathbf{mf}$ for $\mathbf{p}$ in the probability simplex and any scalar α results in $\mathbf{w} = \mathbf{p}$, so that the entire

probability simplex is thus obtained from A. The conditions on $\mathbf{mf}$ and the ~~emissions stopped, σ_i~~ imply that $\mathbf{x}$ has non-zero probability of lying in A, and hence the algorithm has non-zero probability of terminating on each iteration. Because each iteration is an i.i.d. Bernoulli trial, the algorithm thus terminates with probability one.

The two simulations differ in the assigned mixing state of the initial aerosol populations and the aerosol emissions. For the measurement-constrained case we distinguish between rBC-rich and ~~the evolution of the aerosol population was tracked for another 12 . More details can be found in the SI, section 7.~~ HOA-rich particle classes, as the observations indicate. Both classes consist of two modes, which amounts to four modes in total, as listed in Table S1 in the Supplement. Note that the modes BC1 and HOA1 have the same geometric mean diameter and geometric standard deviation, but differ in their abundance and their emission rate, respectively. The same applies to modes BC2 and HOA2. This specific choice is guided by the observations as shown in Table S1 in the Supplement.

~~From the information on per-particle composition it is straightforward to calculate per-particle properties~~ For the uniform case only two modes are prescribed, with the same geometric mean diameter and standard deviation as modes BC1/HOA1 and BC2/HOA2, respectively (Table S2 in the Supplement). The mass fractions of BC and HOA in these two modes are identical, and they are equal to the mass fractions of the bulk concentrations for the measurement constrained case. Hence the uniform case represents conditions for which the bulk mass concentrations and the size distribution are the same as for the measurement-constrained case, but for which the detailed mixing state information is not available. A comparison of the two cases therefore quantifies the importance of mixing state information at emission for properties of interest, such as ~~hygroscopicity (Riemer et al., 2010; Zaveri et al., 2010; Ching et al., 2012; Tian et al., 2014; Fierce et al., 2013), optical properties (Zaveri et al., 2010), and particle reactivity (Kaiser et al., 2011), and to reconstruct the~~ optical properties ~~of the entire population~~and CCN activation properties.

Figure S10 in the Supplement shows the temporal evolution of the bulk aerosol species over the course of the 24 h simulation. The primary species black carbon and organic carbon increase initially owing to emissions, and then decrease after emissions are discontinued at $t = 12$ h as a result of dilution with the background. The model simulations also show the production of inorganic and organic secondary aerosol species, which condense on the primary particles, continuously modifying the composition of each particle in the aerosol population. Not shown on this figure is the aerosol water content. While the particles start out dry, they take up water around $t = 6$ h when nitrate formation begins.

We calculate the optical properties for ambient conditions (including aerosol water content) at a wavelength of 550 nm and the critical supersaturations of each particle in a post processing step according to Zaveri et al. (2010). For the optical properties we assume spherical particles with a "core-and-shell" configuration in which BC forms the particle core and the other substances compose the shell. We then use Mie calculations (Ackerman and Toon, 1981) to determine the extinction and

scattering cross sections for each particle in the population. From these values, the volume extinction, scattering, and absorption coefficients can be reconstructed. Note that we assume all primary and secondary organic substances to be non-absorbing, hence we do not consider any effects due to brown carbon.

To determine the critical supersaturations, we employ κ-Köhler theory (see Zaveri et al. (2010) for details). Based on the critical supersaturation values of each particle in the population, we construct CCN spectra, as shown in Figure S11 in the Supplement for different times throughout the simulation. As the simulation progresses, the CCN/CN fraction at low values of critical supersaturation increases, since the the particles become more hygroscopic due to the condensation of secondary aerosol material. Since both primary organic carbon ($\kappa = 0.001$) and black carbon ($\kappa = 0$) are model species with similar and low hygroscopicity parameters, the differences between the uniform case and the measurement-constrained case are expected to be small, and the two CCN spectra are almost indistinguishable, as we will show in Section 3.3.

3 Results and discussion

3.1 Two classes of fresh black carbon particles

Based on single particle SP-AMS measurements ~~and using a particle categorization procedure and clustering algorithm described in our previous work (Lee et al., 2015a),~~ in both roadside and non-roadside studies, we identified two types of particles originating from vehicle exhaust~~are identified in both roadside and non-roadside studies (Figure 1and S1);~~ , which are primarily composed of refractory black carbon (rBC) and hydrocarbon-like organic aerosol (Fig. 1a – d). One type is dominated by HOA mass (referred to as the "HOA-rich~~and~~ " particle class) and the other is dominated by rBC ("rBC-rich~~particle classes~~" particle class). The mass spectra of HOA-rich particles (~~Figure 1a~~ Fig. 1a and c) exhibit fragmentation patterns associated with hydrocarbon structures (e.g., m/z 43 ($C_3H_7^+$), 57 ($C_4H_9^+$), 71 ($C_5H_{11}^+$)), and are consistent with previous aerosol mass spectrometer observations of gasoline/diesel vehicle exhaust and unburned lubricating oil (Massoli et al., 2012; Canagaratna et al., 2004; Mohr et al., 2009). In conjunction with differences in mass spectra, clear differences in particle size distributions (Fig. 2c and d) demonstrate that the division of traffic-related rBC-containing particles into HOA-rich and rBC-rich classes is physically meaningful.

The average mass fractions of rBC (mf_{rBC}) in HOA-rich particles during the non-roadside and roadside studies are ~~very~~ low: 0.03 and 0.05, respectively. The narrow distribution of ~~mf_{rBC} (Figure 3aand Figure S1b~~mf_{rBC} (Fig. 3a) suggests that most of the HOA-rich particles are either mixed with a small amount of rBC or do not contain detectable rBC mass~~.~~

, while a very small number of particles contain larger mf_{rBC} (Fig. 3, split axis). Mass spectra of rBC-rich particles are dominated by C_x^+ fragments (i.e., m/z 12, 24, 36, 48 and 60 in ~~Figure 1~~Fig. 1b and d) arising from black carbon. Smaller signals associated with HOA-like material in these par-

ticles are similar to the primary organic materials derived from diesel engine exhaust observed in laboratory studies (Sage et al., 2008). In contrast to the HOA-rich particles, ~~Figures 3c and S1d illustrate a range of mf_{rBC}~~ Figure 3c illustrates a wider range of mf_{rBC} values in rBC-rich particles. In the non-roadside and roadside environments the average mf_{rBC} values (± 1 standard deviation) in this particle class are 0.72 (± 0.18) and 0.86 (± 0.14), respectively, highlighting the possibility that condensation and/or coagulation of HOA material on rBC particles might occur within a short time of emission.

The mass fraction of rBC derived from SP-AMS measurements may be best regarded as a lower limit. For the reasons detailed in Sect. 2.1.2, including the potential for incomplete vaporisation and uncertainty in SP-AMS sensitivity to rBC coating materials, mf_{rBC} values presented here may be underestimated. A 50 % overestimation in the mass of HOA would increase mf_{rBC} in rBC-rich particles to 0.85 (± 0.16) and 0.92 (± 0.10) in the non-roadside and roadside studies, respectively (Fig. 3c, dashed lines). In addition to these uncertainties, in the roadside study only rBC-containing particles are detected by the SP-AMS, while in the non-roadside study it is possible that the HOA-rich class includes HOA particles that do not contain rBC (i.e., "externally mixed" HOA).

3.1.1 Differences in particle coating thickness

With single particle detection capability, SP-AMS observations can be used to quantify the thickness of non-refractory particulate matter on individual rBC-containing particles. This calculation focuses only on determining the thickness of HOA coating derived from traffic emissions; however, oxygenated organic aerosol (OOA), biomass burning organic aerosol (BBOA) and secondary inorganic species were mixed with rBC in more aged accumulation mode particles in these urban studies and a similar calculation could be carried out for these particle classes (Lee et al., 2015a, b).

We assume a core-shell structure in order to determine the thickness of HOA coating on fresh rBC-containing particles. In addition, we assume a spherical rBC core, a uniform thickness of coating, and an HOA density of 0.9 $\mathrm{g\,cm^{-3}}$. To simulate the effect of the fractal structure of ambient rBC, the effective density of rBC ($\rho_{\mathrm{eff,rBC}}$) was varied between 0.3 and 1.3 $\mathrm{g\,cm^{-3}}$; values which have been observed for laboratory soot standards and engine exhaust (Maricq and Ning, 2004; Gysel et al., 2011). Figure 4 presents the two-dimensional histograms (mf_{rBC} vs. particle aerodynamic diameter, d_{va}) of rBC-rich and HOA-rich particles identified by cluster analysis in the two urban studies, with calculated coating thickness curves overlaid for comparison (dashed lines). The coating thickness is relatively insensitive to variations in $\rho_{\mathrm{eff,rBC}}$ (Fig. 4, dashed lines).

These observations demonstrate that rBC-rich particles are only very thinly coated with HOA-material, as compared to HOA-rich particles that have only very small rBC inclusions (~~SI section~~ Fig. 4). Here we use two specific examples to illustrate that the coating thickness on HOA-rich and rBC-rich particles can vary significantly. First, a 200 nm (d_{va}) rBC-rich particle (i.e., physical particle diameter ~245 nm, assuming $\rho_{\mathrm{eff,rBC}} = 0.8\,\mathrm{g\,cm^{-3}}$) with 72 – 86 % rBC by mass (the average

mf_{rBC} of rBC-rich particles) would be covered by a 5 – 11 nm HOA coating. Second, a 300 nm (d_{va}) HOA-rich particle (i.e., physical particle diameter ~335 nm, assuming $\rho_{eff,rBC}$ = 0.8 g cm^{-3}) that co-exists with a small amount of rBC mass (3 ~~, Figure S2)~~ – 5 % by mass, the average mf_{rBC} of HOA-rich particles) has an rBC core size of 108 – 119 nm and a thick HOA coating (108 – 113 nm).

3.2 Black carbon mass is dominated by black carbon rich particles

Single particle measurements provide direct insight into mixing state at an individual particle level; however, single particle detection has an inherent bias towards large particle sizes because light scattering triggers particle detection (Lee et al., 2015a; Cross et al., 2009; Freutel et al., 2013; Liu et al., 2013b). Ensemble size distributions of rBC peaked at ~100 nm in both roadside and non-roadside studies indicating that fresh rBC-containing particles emitted from vehicle exhaust are small (~~Figure 2s and S3a~~Fig. 2a and b). Smaller rBC-containing particles fall below the lower size limit of single particle detection (~~Figure 2b and S3b~~Fig. 2c and d). Therefore, single particle observations do not necessarily quantify mixing state at the population level. To provide a complementary view of rBC mixing state we turn to ensemble measurements from the roadside study where only rBC-containing particles were detected in the SP-AMS. Ensemble measurements better represent mixing state on a population basis compared to single particle observations, because they cover a wider range of particle size (i.e., 80 – 1000 nm vacuum aerodynamic diameter, d_{va}).

By measuring very close to a busy road, ensemble SP-AMS observations of rBC and organic aerosol enabled the analysis of more than one hundred vehicle exhaust plumes over the course of the roadside study (~~Figure~~ Fig. 5a and b). Positive matrix factorization (PMF) (Zhang et al., 2011; Ulbrich et al., 2009) indicates three major sources of ~~rBC and organic~~ rBC-containing aerosol in the roadside environment: transported biomass burning (BBOA), regional background (OOA), and traffic emissions comprised of two PMF factors (HOA-rich and rBC-rich factors, ~~Figure 5c-f).~~ Fig. 5c – f). Inorganic species evident in the bulk aerosol size distributions (Fig. 2a and b) are largely associated with OOA and BBOA factors, while the traffic-related factors contain the majority of rBC and HOA (Lee et al., 2015a, b). Mass spectra of all four PMF factors and a discussion of selection of the number of factors is presented in ~~SI section 5.~~ Supplement Sect. 2. Not previously observed with an AMS, the ~~HOA-~~ HOA-rich and rBC-rich factors represent two types of vehicle exhaust plumes with different amounts of rBC and HOA (~~Figure 1b and e~~ Fig. 1e and f). The ~~mf_{rBC} of HOA-~~ mf_{rBC} of HOA-rich and rBC-rich factors are 0.16 and 0.75, respectively. High-time resolution SP-AMS measurements (~~Figure~~ Fig. 6) also demonstrated varying organic and rBC levels in vehicle plumes (~~Figure 1e and f~~Fig. 1g and h), with corresponding differences in optical properties (SSA at 405 ~~nm~~ nm) indicating that rBC-rich plumes were more highly absorbing. The origin of different plume types at this site has been characterized through long-term measurements, and is related to a variety of engine types, operating conditions and pollution control features (Wang et al., 2015).

~~Figure 1b and e show the mass spectra of HOA.~~ Mass spectra of HOA-rich and rBC-rich PMF factors ~~, which~~ (Fig. 1e and f) are strikingly similar to the mass spectra of ~~HOA.~~ HOA-rich and rBC-rich particle classes identified in the single particle measurements (~~Figure 1a~~ Fig. 1c and d), validating the division of traffic emissions into the two factors observed here. The single particle and ensemble mass spectra show some differences. First, the HOA-rich factor has a larger rBC content compared to the HOA-rich particle class; second, the rBC-rich factor contains higher CO^+ and CO_2^+ signals compared to the rBC-rich particle class (inserts of ~~Figures~~ Figs. 1d, e and f). The latter difference arises because highly oxygenated organic fragments (m/z 28 (CO^+) and 44 (CO_2^+)) were excluded in the single particle analysis due to interference of air signals in UMR spectra ~~(Lee et al., 2015a). The former difference likely arises because of SP-AMS sensitivity to rBCand~~ (Lee et al., 2015a). Differences in mf_{rBC} between single particle and ensemble measurements, especially for HOA-rich particles that contain a small amount of rBC, could be due to the probability of rBC detection in a single particle ~~(Lee et al., 2015a)~~such that single particle mf_{rBC} may be underestimated relative to ensemble mf_{rBC} Lee et al. (2015a).

With support of direct measurements of single particle mixing state, this work presents the first interpretation of ensemble AMS results in terms of rBC and HOA mixing state. Using the intensity of the two traffic-related factors in plumes (~~Figure 5d~~ Fig. 5e and f), we estimate that rBC-rich particles account for ~90 % of the observed total traffic-related rBC mass (~~Figure~~ Fig. 3d). In a similar manner, we estimate that ~60 % of the total HOA mass is due to HOA-rich particles (~~Figure~~ Fig. 3b). Purple dashed lines shown in Figure 3b and d represent the inclusion of all CO_x^+ fragments (due to surface functionality of ambient rBC (Corbin et al., 2014)) in the calculation of rBC mass (see ~~SI section~~ Supplement Sect. 1), providing similar results. ~~Red dashed~~ Dashed lines in Figure 3a, b and c represent the effect of a 50 % overestimation of HOA mass (see Supplement Sect. 1), again providing similar results.

3.3 Black carbon mixing state at emission impacts modelled optical properties

These novel single particle and ensemble observations of rBC mixing state were used to initialize the particle-resolved aerosol box model PartMC-MOSAIC (~~SI section 6 and 7~~see Section 2.3) (Zaveri et al., 2008; Riemer et al., 2009), which simulates the evolution of aerosol due to condensation and coagulation in an idealized urban setting. ~~We~~ As described in Section 2.3, we simulate two cases to isolate the impact of mixing state of rBC emissions on aerosol properties. First, a uniform mixing state case in which all particles are assigned identical composition at emission (measured average mf_{rBC}), and second, a measurement-constrained mixing state case where mf_{rBC} is prescribed directly from our mixing state observations. The evolution of dry mf_{rBC} over a 24 h period is illustrated in Figure 7a and b for the two cases. As ageing proceeds mf_{rBC} shifts to lower values, but in the uniform initial composition case no particles ever have mf_{rBC} larger than ~45 %. Note that the bulk aerosol composition and number size distributions are identical in the two cases (~~Figure~~ Fig. S10

in the Supplement), and any differences in optical properties arise only due to the distribution of aerosol components amongst the particles.

Optical properties are determined for each particle in the population using Mie calculations and assuming a core-shell structure. We acknowledge that the underlying assumptions of Mie calculations may not be appropriate for rBC-containing aerosol in the real atmosphere (e.g., Adachi et al., 2011; Scarnato et al., 2013), which is often not spherical and may not exhibit a core-shell configuration (e.g., China et al., 2015). In particular, the enhancement of rBC absorption due to non-absorbing coatings may be overestimated (Cappa et al., 2012; Healy et al., 2015), except in situations where rBC sources and ageing promote extensive coating (Liu et al., 2015; China et al., 2015). However, Mie calculations are commonly applied in regional and global models (Chung and Seinfeld, 2005; Zhao et al., 2013; Fast et al., 2006) to estimate optical properties, and we therefore include this comparison to illustrate the sensitivity to mixing state.

Consistent with previous studies (e.g., Zaveri et al., 2010; Matsui et al., 2013), we observe a difference in volume absorption and scattering coefficients (B_{abs} and B_{scat}, Fig. 7c), and a resulting increase of 0.1 in SSA from the uniform mixing state to the measurement-constrained case that is present during the emission period in the simulation and, notably, persists throughout ageing (Fig. 7d). Note that a direct comparison between measured and modelled SSA is not valid since we measure SSA of the bulk aerosol population and model it only for a subset of this population (i.e., the rBC containing particles). No significant differences in calculated cloud condensation nuclei activity were observed in these simulations (Fig. S11 in the Supplement), owing to the very similar hygroscopicity of rBC and HOA species. Calculations of aerosol DRF are very sensitive to changes in SSA (McComiskey et al., 2008) (e.g., uncertainties in SSA on the order of only 0.02 can result in a DRF uncertainty of $1\,\mathrm{W\,m^{-2}}$ for a particular particle type (Chin et al., 2009)), illustrating the importance of accurately measuring and simulating mixing state for calculating climatologically relevant aerosol properties.

4 Conclusions

We present mass-based measurements of the mixing state of black carbon-containing aerosol, using a soot-particle aerosol mass spectrometer, from traffic emissions in an urban environment. Observations from single particle mass spectrometry indicate that rBC co-exists with hydrocarbon-like organic aerosol (HOA) in two distinct particle types; those containing a larger mass fraction of rBC, and those containing a larger mass fraction of HOA. Source apportionment of ensemble mass spectral observations using positive matrix factorization also indicates two types of rBC-containing aerosol related to traffic: rBC-rich and HOA-rich aerosol, validated by single particle observations. Ensemble measurements expand the particle size range over which mixing state can be investigated, providing a better insight into the mixing state of the particle population and indicating that approx-

imately 90 % of rBC mass resides in rBC-rich particles. These measurements were used to drive the particle-resolved aerosol box model, PartMC-MOSAIC. Our results indicate an increase in SSA of ~ 0.1 when mixing state at the point of emission is treated accurately in the model, compared to the assumption of uniform mixing state. The approach described here for quantitative assessment of black carbon mixing state from traffic can also be used to assess mixing state from other sources, and to explore the evolution of mixing state during atmospheric processing. Such measurements will be crucial to drive accurate model assessment of black carbon climate impacts on a broader scale.

Acknowledgements. This work was financially supported by Natural Sciences and Engineering Research Council (NSERC) of Canada, Environment Canada, the Canada Foundation for Innovation and the Marie Curie Action FP7-PEOPLE-IOF-2011 (Project: CHEMBC, No. 299755). N.R. and M.W. acknowledge funding from the Department of Energy under Grant DOE DE-SC0011771.

References

Ackerman, T. and Toon, O.: Absorption of visible radiation in atmospheres containing mixtures of absorbing and nonabsorbing particles, Applied Optics, 20, 3661–3668, doi:10.1364/AO.20.003661, 1981.

Adachi, K. and Buseck, P. R.: Changes of ns-soot mixing states and shapes in an urban area during CalNex, Journal of Geophysical Research-Atmospheres, 118, 3723–3730, 2013.

Adachi, K., Freney, E. J., and Buseck, P. R.: Shapes of internally mixed hygroscopic aerosol particles after deliquescence, and their effect on light scattering, Geophysical Research Letters, 38, L13 804, doi:10.1029/2011GL047540, L13804, 2011.

Adachi, K., Zaizen, Y., Kajino, M., and Igarashi, Y.: Mixing state of regionally transported soot particles and the coating effect on their size and shape at a mountain site in Japan, Journal of Geophysical Research-Atmospheres, 119, 5386–5396, doi:10.1002/2013JD020880, 2014.

Arnott, W. P., Moosmüller, H., Rogers, C. F., Jin, T., and Bruch, R.: Photoacoustic spectrometer for measuring light absorption by aerosol: instrument description, Atmospheric Environment, 33, 2845 – 2852, doi:http://dx.doi.org/10.1016/S1352-2310(98)00361-6, http://www.sciencedirect.com/science/article/pii/S1352231098003616, 1999.

Bond, T. C., Doherty, S. J., Fahey, D. W., Forster, P. M., Berntsen, T., DeAngelo, B. J., Flanner, M. G., Ghan, S., Kärcher, B., Koch, D., Kinne, S., Kondo, Y., Quinn, P. K., Sarofim, M. C., Schultz, M. G., Schulz, M., Venkataraman, C., Zhang, H., Zhang, S., Bellouin, N., Guttikunda, S. K., Hopke, P. K., Jacobson, M. Z., Kaiser, J. W., Klimont, Z., Lohmann, U., Schwarz, J. P., Shindell, D., Storelvmo, T., Warren, S. G., and Zender, C. S.: Bounding the role of black carbon in the climate system: A scientific assessment, Journal of Geophysical Research-Atmospheres, 118, 5380–5552, 2013.

Canagaratna, M. R., Jayne, J. T., Ghertner, D. A., Herndon, S., Shi, Q., Jimenez, J. L., Silva, P. J., Williams, P., Lanni, T., Drewnick, F., Demerjian, K. L., Kolb, C. E., and Worsnop, D. R.: Chase studies of particulate emissions from in-use New York City vehicles, Aerosol Science and Technology, 38, 555–573, 2004.

Cappa, C. D., Onasch, T. B., Massoli, P., Worsnop, D. R., Bates, T. S., Cross, E. S., Davidovits, P., Hakala, J., Hayden, K. L., Jobson, B. T., Kolesar, K. R., Lack, D. A., Lerner, B. M., Li, S. M., Mellon, D., Nuaaman, I., Olfert, J. S., Petaja, T., Quinn, P. K., Song, C., Subramanian, R., Williams, E. J., and Zaveri, R. A.: Radiative Absorption Enhancements Due to the Mixing State of Atmospheric Black Carbon, Science, 337, 1078–1081, 2012.

Chan, T. W., Brook, J. R., Smallwood, G. J., and Lu, G.: Time-resolved measurements of black carbon light absorption enhancement in urban and near-urban locations of southern Ontario, Canada, Atmospheric Chemistry and Physics, 11, 10 407–10 432, doi:10.5194/acp-11-10407-2011, http://www.atmos-chem-phys.net/11/10407/2011/, 2011.

Chin, M., Kahn, R., Rind, D., Feingold, G., Schwartz, S., and DeCola, P.: Atmospheric Aerosol Properties and Climate Impacts, A Report by the U.S. Climate Change Science Program and the Subcommittee on Global Change Research, Tech. Rep. SAP 2.3, NASA, Washington, D.C., 2009.

China, S., Salvadori, N., and Mazzoleni, C.: Effect of Traffic and Driving Characteristics on Morphology of Atmospheric Soot Particles at Freeway On-Ramps, Environmental Science and Technology, 48, 3128–3135, 2014.

China, S., Scarnato, B., Owen, R., Zhang, B., Ampadu, M., Kumar, S., Dzepina, K., Dziobak, M., Fialho, P., Perlinger, J., Hueber, J., D. Helmig, Mazzoleni, L., and Mazzoleni, C.: Morphology and mixing state of aged soot particles at a remote marine free troposphere site: Implications for optical properties, Geophysical Research Letters, 42, 1243–1250, 2015.

Ching, J., Riemer, N., and West, M.: Impacts of black carbon mixing state on black carbon nucleation scavenging: Insights from a particle-resolved model, Journal of Geophysical Research-Atmospheres, 117, doi:10.1029/2012JD018269, 2012.

Chirico, R., DeCarlo, P. F., Heringa, M. F., Tritscher, T., Richter, R., Prevot, A. S. H., Dommen, J., Weingartner, E., Wehrle, G., Gysel, M., Laborde, M., and Baltensperger, U.: Impact of aftertreatment devices on primary emissions and secondary organic aerosol formation potential from in-use diesel vehicles: results from smog chamber experiments, Atmospheric Chemistry and Physics, 10, 11 545–11 563, 2010.

Chung, S. H. and Seinfeld, J. H.: Climate response of direct radiative forcing of anthropogenic black carbon, Journal of Geophysical Research: Atmospheres, 110, doi:10.1029/2004JD005441, 2005.

Corbin, J. C., Sierau, B., Gysel, M., Laborde, M., Keller, A., Kim, J., Petzold, A., Onasch, T. B., Lohmann, U., and Mensah, A.: Mass spectrometry of refractory black carbon particles from six sources: carbon-cluster and oxygenated ions, Atmospheric Chemistry and Physics, 14, 2591–2603, 2014.

Cross, E. S., Onasch, T. B., Canagaratna, M., Jayne, J. T., Kimmel, J., Yu, X. Y., Alexander, M. L., Worsnop, D. R., and Davidovits, P.: Single particle characterization using a light scattering module coupled to a time-of-flight aerosol mass spectrometer, Atmospheric Chemistry and Physics, 9, 7769–7793, 2009.

Dallmann, T., Onasch, T. B., Kirchstetter, T. W., Worton, D., Fortner, E. C., Herndon, S. C., Wood, E. C., Franklin, J. P., Worsnop, D. R., Goldstein, A., and Harley, R.: Characterization of particulate matter emission from on-road gasoline and diesel vehicles using a soot particle aerosol mass spectrometer, Atmospheric Chemistry and Physics, 14, 7585–7599, 2014.

DeVille, R., Riemer, N., and West, M.: Weighted Flow Algorithms (WFA) for stochastic particle coagulation, Journal of Computational Physics, 230, 8427–8451, 2011.

Fast, J. D., Gustafson, W. I., Easter, R. C., Zaveri, R. A., Barnard, J. C., Chapman, E. G., Grell, G. A., and Peckham, S. E.: Evolution of ozone, particulates, and aerosol direct radiative forcing in the vicinity of Houston using a fully coupled meteorology-chemistry-aerosol model, Journal of Geophysical Research: Atmospheres, 111, doi:10.1029/2005JD006721, 2006.

Fierce, L., Riemer, N., and Bond, T. C.: When is cloud condensation nuclei activity sensitive to particle characteristics at emission?, Journal of Geophysical Research: Atmospheres, 118, 13,476–13,488, doi:10.1002/2013JD020608, 2013.

Flowers, B. A., Dubey, M. K., Mazzoleni, C., Stone, E. A., Schauer, J. J., Kim, S.-W., and Yoon, S. C.: Optical-chemical-microphysical relationships and closure studies for mixed carbonaceous aerosols observed at Jeju Island; 3-laser photoacoustic spectrometer, particle sizing, and filter analysis, Atmospheric Chemistry and Physics, 10, 10 387–10 398, doi:10.5194/acp-10-10387-2010, http://www.atmos-chem-phys.net/10/10387/2010/, 2010.

Freutel, F., Drewnick, F., Schneider, J., Klimach, T., and Borrmann, S.: Quantitative single-particle analysis with the Aerodyne aerosol mass spectrometer: development of a new classification algorithm and its application to field data, Atmospheric Measurement Techniques, 6, 3131–3145, 2013.

Gysel, M., Laborde, M., Olfert, J. S., Subramanian, R., and Groehn, A. J.: Effective density of Aquadag and fullerene soot black carbon reference materials used for SP2 calibration, Atmospheric Measurement Techniques, 4, 2851–2858, 2011.

Healy, R. M., Sciare, J., Poulain, L., Kamili, K., Merkel, M., Mueller, T., Wiedensohler, A., Eckhardt, S., Stohl, A., Sarda-Esteve, R., McGillicuddy, E., O'Connor, I. P., Sodeau, J. R., and Wenger, J. C.: Sources and mixing state of size-resolved elemental carbon particles in a European megacity: Paris, Atmospheric Chemistry and Physics, 12, 1681–1700, 2012.

Healy, R. M., Wang, J. M., Jeong, C.-H., Lee, A. K. Y., Willis, M. D., Jaroudi, E., Zimmerman, N., Hilker, N., Murphy, M., Eckhardt, S., Stohl, A., Abbatt, J. P. D., Wenger, J. C., and Evans, G. J.: Light-absorbing properties of ambient black carbon and brown carbon from fossil fuel and biomass burning sources, Journal of Geophysical Research: Atmospheres, 120, 6619–6633, doi:10.1002/2015JD023382, 2015.

Jacobson, M. Z.: A physically-based treatment of elemental carbon optics: Implications for global direct forcing of aerosols, Geophysical Research Letters, 27, 217–220, doi:10.1029/1999GL010968, 2000.

Jacobson, M. Z.: Strong radiative heating due to the mixing state of black carbon in atmospheric aerosols, Nature, 409, 695–697, 2001.

Jimenez, J. L., Jayne, J. T., Shi, Q., Kolb, C. E., Worsnop, D. R., Yourshaw, I., Seinfeld, J. H., Flagan, R., Zhang, X., Smith, K., Morris, J., and Davidovits, P.: Ambient aerosol sampling using the Aerodyne Aerosol Mass Spectrometer, Journal of Geophysical Research-Atmospheres, 108, doi:10.1029/2001JD001213, 2003.

Johnson, K. S., Zuberi, B., Molina, L. T., Molina, M. J., Iedema, M. J., Cowin, J. P., Gaspar, D. J., Wang, C., and Laskin, A.: Processing of soot in an urban environment: case study from the Mexico City Metropolitan Area, Atmospheric Chemistry and Physics, 5, 3033–3043, 2005.

Kaiser, J. C., Riemer, N., and Knopf, D. A.: Detailed heterogeneous oxidation of soot surfaces in a particle-resolved aerosol model, Atmospheric Chemistry and Physics, 11, 4505–4520, 2011.

Knox, A., Evans, G. J., Brook, J. R., Yao, X., Jeong, C. H., Godri, K. J., Sabaliauskas, K., and Slowik, J. G.: Mass Absorption Cross-Section of Ambient Black Carbon Aerosol in Relation to Chemical Age, Aerosol Science and Technology, 43, 522–532, 2009.

Kuwata, M., Kondo, Y., and Takegawa, N.: Critical condensed mass for activation of black carbon as cloud condensation nuclei in Tokyo, Journal of Geophysical Research-Atmospheres, 114, doi:10.1029/2009JD012086, 2009.

Laborde, M., Crippa, M., Tritscher, T., Juranyi, Z., Decarlo, P. F., Temime-Roussel, B., Marchand, N., Eckhardt, S., Stohl, A., Baltensperger, U., Prevot, A. S. H., Weingartner, E., and Gysel, M.: Black carbon physical properties and mixing state in the European megacity Paris, Atmospheric Chemistry and Physics, 13, 5831–5856, 2013.

Lack, D. A., Langridge, J. M., Bahreini, R., Cappa, C. D., Middlebrook, A. M., and Schwarz, J. P.: Brown carbon and internal mixing in biomass burning particles, Proceedings of the National Academy of Sciences of the United States of America, 109, 14 802–14 807, 2012.

Lee, A. K. Y., Willis, M. D., Healy, R. M., Onasch, T. B., and Abbatt, J. P. D.: Mixing state of carbonaceous aerosol in an urban environment: Single particle characterization using a soot particle aerosol mass spectrometer (SP-AMS), Atmospheric Chemistry and Physics, 15, 1823–1841, 2015a.

Lee, A. K. Y., Willis, M. D., Healy, R. M., Wang, J. M., Jeong, C.-H., Wenger, J. C., Evans, G. J., and Abbatt, J. P. D.: Single particle characterization of biomass burning organic aerosol (BBOA): evidence for non-uniform mixing of high molecular weight organics and potassium, Atmospheric Chemistry and Physics Discussions, 15, 32 157–32 183, doi:10.5194/acpd-15-32157-2015, http://www.atmos-chem-phys-discuss.net/15/32157/2015/, 2015b.

Liu, D., Allan, J., Whitehead, J., Young, D., Flynn, M., Coe, H., McFiggans, G., Fleming, Z. L., and Bandy, B.: Ambient black carbon particle hygroscopic properties controlled by mixing state and composition, Atmospheric Chemistry and Physics, 13, 2015–2029, 2013a.

Liu, D., Allan, J. D., Young, D. E., Coe, H., Beddows, D., Fleming, Z. L., Flynn, M. J., Gallagher, M. W., Harrison, R. M., Lee, J., Prevot, A. S. H., Taylor, J. W., Yin, J., Williams, P. I., and Zotter, P.: Size distribution, mixing state and source apportionment of black carbon aerosol in London during wintertime, Atmospheric Chemistry and Physics, 14, 10 061–10 084, 2014.

Liu, P. F., Zhao, C. S., Göbel, T., Hallbauer, E., Nowak, A., Ran, L., Xu, W. Y., Deng, Z. Z., Ma, N., Mildenberger, K., Henning, S., Stratmann, F., and Wiedensohler, A.: Hygroscopic properties of aerosol particles at high relative humidity and their diurnal variations in the North China Plain, Atmospheric Chemistry and Physics, 11, 3479–3494, doi:10.5194/acp-11-3479-2011, http://www.atmos-chem-phys.net/11/3479/2011/, 2011.

Liu, S., Russell, L. M., Sueper, D. T., and Onasch, T. B.: Organic particle types by single-particle measurements using a time-of-flight aerosol mass spectrometer coupled with a light scattering module, Atmospheric Measurement Techniques, 6, 187–197, 2013b.

Liu, S., Aiken, A. C., Gorkowski, K., Dubey, M., Cappa, C. D., Williams, L. R., Herndon, S. C., Massoli, P., Fortner, E. C., Chhabra, P., Brooks, W., Onasch, T. B., Jayne, J. T., Worsnop, D., China, S., Sharma, N., Mazzoleni, C., Xu, L., Ng, N., Liu, D., Allan, J. D. Lee, J., Fleming, Z. L. Mohr, C., Zotter, P., Szidat, P., and Prevot, A. S. H.: Enhanced light absorption by mixed source black and brown carbon particles in UK winter, Nature Communications, 6, doi:10.1038/ncomms9435, 2015.

Maricq, M. M. and Ning, X.: The effective density and fractal dimension of soot particles from premixed flames and motor vehicle exhaust, Journal of Aerosol Science, 35, 1251–1274, 2004.

Massoli, P., Fortner, E. C., Canagaratna, M. R., Williams, L. R., Zhang, Q., Sun, Y., Schwab, J. J., Trimborn, A., Onasch, T. B., Demerjian, K. L., Kolb, C. E., Worsnop, D. R., and Jayne, J. T.: Pollution Gradients and Chemical Characterization of Particulate Matter from Vehicular Traffic near Major Roadways: Results from the 2009 Queens College Air Quality Study in NYC, Aerosol Science and Technology, 46, 1201–1218, 2012.

Matsui, H., Koike, M., Kondo, Y., Moteki, N., Fast, J. D., and Zaveri, R. A.: Development and validation of a black carbon mixing state resolved three-dimensional model: Aging processes and radiative impact, Journal of Geophysical Research: Atmospheres, 118, 2304–2326, doi:10.1029/2012JD018446, 2013.

McComiskey, A., Schwartz, S., Schmid, B., Guan, H., Lewis, E., Ricchiazzi, P., and Ogren, J.: Direct aerosol forcing: Calculation from observables and sensitivities to inputs, Journal of Geophysical Research, 113, doi:10.1029/2007JD009170, 2008.

McMeeking, G. R., Good, N., Petters, M. D., McFiggans, G., and Coe, H.: Influences on the fraction of hydrophobic and hydrophilic black carbon in the atmosphere, Atmospheric Chemistry and Physics, 11, 5099–5112, 2011a.

McMeeking, G. R., Morgan, W. T., Flynn, M., Highwood, E. J., Turnbull, K., Haywood, J., and Coe, H.: Black carbon aerosol mixing state, organic aerosols and aerosol optical properties over the United Kingdom, Atmospheric Chemistry and Physics, 11, 9037–9052, 2011b.

Michelotti, M., Heath, M., and West, M.: Binning for efficient stochastic multiscale particle simulations, Multiscale Model Simulations, 11, 1071–1096, 2013.

Moffet, R. C. and Prather, K. A.: In-situ measurements of the mixing state and optical properties of soot with implications for radiative forcing estimates, Proceedings of the National Academy of Sciences of the United States of America, 106, 11 872–11 877, 2009.

Mohr, C., Huffman, J. A., Cubison, M. J., Aiken, A. C., Docherty, K. S., Kimmel, J. R., Ulbrich, I. M., Hannigan, M., and Jimenez, J. L.: Characterization of Primary Organic Aerosol Emissions from Meat Cooking, Trash Burning, and Motor Vehicles with High-Resolution Aerosol Mass Spectrometry and Comparison with Ambient and Chamber Observations, Environmental Science and Technology, 43, 2443–2449, 2009.

Moosmüller, H., Chakrabarty, R., and Arnott, W.: Aerosol light absorption and its measurement: A review, Journal of Quantitative Spectroscopy and Radiative Transfer, 110, 844 – 878, doi:http://dx.doi.org/10.1016/j.jqsrt.2009.02.035, http://www.sciencedirect.com/science/article/pii/S0022407309000879, light Scattering: Mie and More Commemorating 100 years of Mie's 1908 publication, 2009.

Moteki, N., Kondo, Y., Miyazaki, Y., Takegawa, N., Komazaki, Y., Kurata, G., Shirai, T., Blake, D. R., Miyakawa, T., and Koike, M.: Evolution of mixing state of black carbon particles: Aircraft measurements over the western Pacific in March 2004, Geophysical Research Letters, 34, doi:10.1029/2006GL028943, 2007.

Onasch, T. B., Trimborn, A., Fortner, E. C., Jayne, J. T., Kok, G. L., Williams, L. R., Davidovits, P., and Worsnop, D. R.: Soot Particle Aerosol Mass Spectrometer: Development, Validation, and Initial Application, Aerosol Science and Technology, 46, 804–817, 2012.

Oshima, N., Koike, M., Zhang, Y., and Kondo, Y.: Aging of black carbon in outflow from anthropogenic sources using a mixing state resolved model: 2. Aerosol optical properties and cloud condensation nuclei activities, Journal of Geophysical Research: Atmospheres, 114, doi:10.1029/2008JD011681, http://dx.doi.org/10.1029/2008JD011681, d18202, 2009.

Paatero, P. and Tapper, U.: Positive matrix factorization: A non-negative factor model with optimal utilization of error estimate of data values, Environmetrics, 5, 111–126, 1994.

Ramanathan, V. and Carmichael, G.: Global and regional climate changes due to black carbon, Nature Geoscience, 1, 221–227, 2008.

Riemer, N., West, M., Zaveri, R. A., and Easter, R. C.: Simulating the evolution of soot mixing state with a particle-resolved aerosol model, Journal of Geophysical Research-Atmospheres, 114, doi:10.1029/2008JD011073, 2009.

Riemer, N., West, M., Zaveri, R., and Easter, R.: Estimating soot aging time scales with a particle-resolved aerosol model, Aerosol Science, 41, 143–158, 2010.

Sabaliauskas, K., Jeong, C.-H., , Yao, X., and Evans, G. J.: The application of wavelet decomposition to quantify the local and regional sources of ultrafine particles in cities, Atmospheric Environment, 95, 249–257, doi:http://dx.doi.org/10.1016/j.atmosenv.2014.05.035, 2014.

Sage, A. M., Weitkamp, E. A., Robinson, A. L., and Donahue, N. M.: Evolving mass spectra of the oxidized component of organic aerosol: results from aerosol mass spectrometer analyses of aged diesel emissions, Atmospheric Chemistry and Physics, 8, 1139–1152, 2008.

Scarnato, B. V., Vahidinia, S., Richard, D. T., and Kirchstetter, T. W.: Effects of internal mixing and aggregate morphology on optical properties of black carbon using a discrete dipole approximation model, Atmospheric Chemistry and Physics, 13, 5089–5101, doi:10.5194/acp-13-5089-2013, 2013.

Schneider, J., Weimer, S., Drewnick, F., Borrmann, S., Helas, G., Gwaze, P., Schmid, O., Andreae, M. O., and Kirchner, U.: Mass spectrometric analysis and aerodynamic properties of various types of combustion-related aerosol particles, International Journal of Mass Spectrometry, 258, 37–49, 2006.

Seuper, D.: ToF-AMS analysis software, http://cires.colorado.edu/jimenez-group/ToFAMSResources/ToFSoftware/index.html, 2010.

Shindell, D., Kuylenstierna, J. C. I., Vignati, E., van Dingenen, R., Amann, M., Klimont, Z., Anenberg, S. C., Muller, N., Janssens-Maenhout, G., Raes, F., Schwartz, J., Faluvegi, G., Pozzoli, L., Kupiainen, K., Hoglund-Isaksson, L., Emberson, L., Streets, D., Ramanathan, V., Hicks, K., Oanh, N. T. K., Milly, G., Williams, M., Demkine, V., and Fowler, D.: Simultaneously Mitigating Near-Term Climate Change and Improving Human Health and Food Security, Science, 335, 183–189, 2012.

Shiraiwa, M., Kondo, Y., Moteki, N., Takegawa, N., Sahu, L. K., Takami, A., Hatakeyama, S., Yonemura, S., and Blake, D. R.: Radiative impact of mixing state of black carbon aerosol in Asian outflow, Journal of Geophysical Research-Atmospheres, 113, doi:10.1029/2008JD010546, 2008.

Tian, J., Riemer, N., West, M., Pfaffenberger, L., Schlager, H., and Petzold, A.: Modeling the evolution of aerosol particles in a ship plume using PartMC-MOSAIC, Atmospheric Chemistry and Physics, 14, 5327–5347, 2014.

Toner, S. M., Sodeman, D. A., and Prather, K. A.: Single particle characterization of ultrafine and accumulation mode particles from heavy duty diesel vehicles using aerosol time-of-flight mass spectrometry, Environmental Science and Technology, 40, 3912–3921, 2006.

Tritscher, T., Juranyi, Z., Martin, M., Chirico, R., Gysel, M., Heringa, M. F., DeCarlo, P. F., Sierau, B., Prevot, A. S. H., Weingartner, E., and Baltensperger, U.: Changes of hygroscopicity and morphology during ageing of diesel soot, Environmental Research Letters, 6, doi:10.1088/1748-9326/6/3/034026, 2011.

Ulbrich, I. M., Canagaratna, M. R., Zhang, Q., Worsnop, D. R., and Jimenez, J. L.: Interpretation of organic components from Positive Matrix Factorization of aerosol mass spectrometric data, Atmospheric Chemistry and Physics, 9, 2891–2918, 2009.

Wang, J., Jeong, C.-H., Zimmerman, N., Healy, R. M., Wang, D., Ke, F., and Evans, G.: Plume-based analysis of vehicle fleet air pollutant emissions and the contribution from high emitters, Atmospheric Measurement Techniques, 8, 3263–3275, doi:10.5194/amt-8-3263-2015, 2015.

Willis, M. D., Lee, A. K. Y., Onasch, T. B., Fortner, E. C., WilliamS, L. R., Lambe, A. T., Worsnop, D. R., and Abbatt, J.: Collection efficiency of the soot-particle aerosol mass spectrometer (SP-AMS) for internally mixed particulate black carbon, Atmospheric Measurement Techniques, 7, 4507–4516, 2014.

Zaveri, R., Barnard, J., Easter, R., Riemer, N., and West, M.: Particle-resolved simulation of aerosol size, composition, mixing state, and the associated optical and cloud condensation nuclei activation properties in an evolving urban plume, Journal of Geophysical Research, 115, doi:10.1029/2009JD013616, 2010.

Zaveri, R. A. and Peters, L. K.: A new lumped structure photochemical mechanism for large-scale applications, Journal of Geophysical Research: Atmospheres, 104, 30 387–30 415, doi:10.1029/1999JD900876, 1999.

Zaveri, R. A., Easter, R. C., and Peters, L. K.: A computationally efficient multicomponent equilibrium solver for aerosols (MESA), Journal of Geophysical Research: Atmospheres, 110, doi:10.1029/2004JD005618, 2005a.

Zaveri, R. A., Easter, R. C., and Wexler, A. S.: A new method for multicomponent activity coefficients of electrolytes in aqueous atmospheric aerosols, Journal of Geophysical Research: Atmospheres, 110, doi:10.1029/2004JD004681, 2005b.

Zaveri, R. A., Easter, R. C., Fast, J. D., and L.K., P.: Model for Simulating Aerosol Interactions and Chemistry (MOSAIC), Journal of Geophysical Research, 113, doi:10.1029/2007JD008782, 2008.

Zhang, G., Bi, X., Li, L., Chan, L. Y., Li, M., Wang, X., Sheng, G., Fu, J., and Zhou, Z.: Mixing state of individual submicron carbon-containing particles during spring and fall seasons in urban Guangzhou, China: a case study, Atmospheric Chemistry and Physics, 13, 4723–4735, 2013.

Zhang, Q., Jimenez, J. L., Canagaratna, M. R., Ulbrich, I. M., Ng, N., Worsnop, D., and Sun, Y.: Understanding atmospheric organic aerosols via factor analysis of aerosol mass spectrometry: A review, Anal. Bioanal. Chem., 401, 3045–3067, doi:10.1007/s00216-011-5355-y, 2011.

Zhang, R. Y., Khalizov, A. F., Pagels, J., Zhang, D., Xue, H. X., and McMurry, P. H.: Variability in morphology, hygroscopicity, and optical properties of soot aerosols during atmospheric processing, Proceedings of the National Academy of Sciences of the United States of America, 105, 10 291–10 296, 2008.

Zhao, C., Liu, X., Qian, Y., Yoon, J., Hou, Z., Lin, G., McFarlane, S., Wang, H., Yang, B., Ma, P.-L., Yan, H., and Bao, J.: A sensitivity study of radiative fluxes at the top of atmosphere to cloud-microphysics and aerosol parameters in the community atmosphere model CAM5, Atmospheric Chemistry and Physics, 13, 10 969–10 987, 2013.

Response to Anonymous Referee # 1

We thank Referee #1 for their thoughtful reading of this manuscript, and for their important questions about the SP-AMS technique. Our responses to specific comments and the corresponding changes to the manuscript are detailed below.

General comments

1. A potentially major technical issue relates to the fact that in the SP-AMS, it is not assured that the particle will completely vaporise. If the particle beam is wider than the laser beam (which given that soot particles are non-spherical, is a distinct possibility), then particles may pass through the "tails" of the laser beam, which may mean that the particles absorb sufficient energy to vaporise the coating of the particle but not the core. This would occur if the peak temperature reached was between the boiling points of the coating of the core, which given this covers a temperature range of thousands of degrees, this is a distinct possibility. Furthermore, a report of this behaviour in diesel emission particles was presented at the most recent AMS users meeting: http://cires1.colorado.edu/jimenezgroup/UsrMtgs/UsersMtg16/JDASPAMSfocusing.pdf. In this paper, the reported population of particles that contained little or no rBC could be attributed to this incomplete vaporisation occurring. It could also give rise to the PMF result as well. The authors should see if they can discount this as a possibility, or failing this, add this possibility in as a caveat. In the worst case that the observation of the "HOA rich" population turns out to be erroneous, what effect would this have on the paper?

Authors' response: The incomplete evaporation of rBC-containing particles in the "tails" of the laser vaporiser is indeed a distinct possibility in our measurements, and is now more explicitly addressed in this paper. As the reviewer states, incomplete vaporisation can take place when the particle beam is wider than the laser beam and this may be the case in our measurements (as mentioned in the Methods section, beam width probe measurements used to estimate the collection efficiency at the roadside site suggest this is the case). We agree that this could certainly have an effect on the mf_{rBC} measured by the SP-AMS; however, we believe we can discount the possibility that the HOA-rich particle class is an artefact caused by incomplete vaporisation because HOA-rich and rBC-rich particle classes have different size distributions in single particle data. If HOA-rich particles arose exclusively from incomplete vaporisation in the edges of the laser, resulting in underestimated mf_{rBC}, we would then expect HOA-rich and rBC-rich particles to have the same size distributions (i.e., the particle-time-of-flight would be the same whether the aerosol was completely or incompletely vaporised). In contrast, we observe that HOA-rich and rBC-rich particle classes have distinct size distributions, supporting the conclusions that their mass spectra arise from different particle types. The importance of the size distributions for interpretation of our results has been highlighted in the revised version of the paper (Section 3.1).

Though we can discount that the HOA-rich population is erroneous, we agree that it is very important to discuss the effect that incomplete vaporisation could

have on the mf_{rBC} values we report. To better address these uncertainties a more detailed description of uncertainties in SP-AMS measurement of mf_{rBC} has been added to Section 2.1 as follows: "...two additional uncertainties in SP-AMS measurements may affect calculation of mf_{rBC}. First, there are uncertainties in the recommended RIE for organic species evaporating from rBC in the SP-AMS of up to ∼50% (Lee et al., 2015; Willis et al., 2014), which could cause an overestimation in the mass of coating material and a corresponding underestimation in mf_{rBC}. Second, it is possible for rBC-containing particles to pass through the edges of the laser vaporizer, thus producing a heating effect sufficient to evaporate some fraction of the coating materials but not evaporate the rBC itself. This effect may also lead to an underestimation in mf_{rBC}. SP-AMS CE and quantification are discussed in further detail in Section 1 of the Supplement." A reference to the cited AMS Users' Meeting report has been added to Section 1 of the Supplement, along with a more detailed discussion of incomplete vaporisation. An explicit reference to Section 2.1 and uncertainties in SP-AMS mf_{rBC} has also been added to Section 3.1 to make clear to the reader that these uncertainties must be considered.

2. Generally speaking, there is perhaps too much of a tendency to put things in the supplementary material. While this would be considered usual practice for a journal with a strict word or page limit, I feel that certain sections of the supplement would be better featured in the main article as they contain information very pertinent to the paper's conclusions. Personally, I would consider that sections 2, 3, 4 and 7 may be suitable for the main article.
Authors' response: Sections 2, 3, 4 and 7 of the Supplement have been added to the main paper, and Figures 1, 2 and 3 have been modified to include data from both the roadside and non-roadside sites. The discussion and figure relating to particle coating thickness estimation have been added to the main text of the paper.

Specific comments

1. Little detail on the PASS-3 operation is presented here. Why was the 405 nm channel used? How was it calibrated? Was any attempt to correct the scattering channel for truncation made?
Authors' response: Omission of this information was an oversight on our part and a new section has been added to the Methods describing the PASS-3, as follows:

"A photoacoustic soot spectrometer (PASS-3, Droplet Measurement Techniques, Boulder, CO) was used to measure aerosol absorption (b_{abs}) and scattering (b_{abs}) coefficients (Mm^{-1}) at 405 and 781 nm. A 532 nm laser is not installed in this particular unit. The PASS determines aerosol absorption (Mm^{-1}) in a cavity which acts as an acoustic resonator. The absorption of incoming radiation heats the particles, which in turn heat the surrounding air in the cavity (Arnott et al., 1999). The aerosol-laden air thus expands, resulting in a pressure disturbance. By modulating the laser power at the resonance frequency of the cavity, the pressure disturbance is amplified and the resulting acoustic wave is measured using a microphone. Light scattering at both wavelengths is concurrently measured using reciprocal nephelom-

etry (Moosmller et al., 2009; Flowers et al., 2010; Chan et al., 2011). Signals were not corrected for truncation; however, it should be noted that total particulate loading is relatively low at this site and saturation was not observed in scattering signals. The instrument was calibrated using a propane soot generator (miniCAST, 6203A, Jing); since a 532 nm laser was not present in this unit an NO_2 calibration was not possible. PASS measurements of the bulk single scattering albedo at 405 nm (selected due to superior signal-to-noise ratio for scattering relative to the 781 nm channel) are used here only to illustrate differences in optical properties in vehicle plumes with varying composition."

2. Regarding the use of PMF, I would request that the authors include the graphs from the rejected solutions as well in the supplement, so as to justify their choice of solution.
Authors' response: The relevant plots for the 2 – factor, 3 – factor and 5 – factor solutions have been added to the Supplement.

References

Arnott, W. P., Moosmller, H., Rogers, C. F., Jin, T., and Bruch, R.: Photoacoustic spectrometer for measuring light absorption by aerosol: instrument description, Atmospheric Environment, 33, 2845 – 2852, doi:http://dx.doi.org/10.1016/S1352-2310(98)00361-6, URL http://www.sciencedirect.com/science/article/pii/S1352231098003616, 1999.

Chan, T. W., Brook, J. R., Smallwood, G. J., and Lu, G.: Time-resolved measurements of black carbon light absorption enhancement in urban and near-urban locations of southern Ontario, Canada, Atmospheric Chemistry and Physics, 11, 10 407–10 432, doi:10.5194/acp-11-10407-2011, URL http://www.atmos-chem-phys.net/11/10407/2011/, 2011.

Flowers, B. A., Dubey, M. K., Mazzoleni, C., Stone, E. A., Schauer, J. J., Kim, S.-W., and Yoon, S. C.: Optical-chemical-microphysical relationships and closure studies for mixed carbonaceous aerosols observed at Jeju Island; 3-laser photoacoustic spectrometer, particle sizing, and filter analysis, Atmospheric Chemistry and Physics, 10, 10 387–10 398, doi:10.5194/acp-10-10387-2010, URL http://www.atmos-chem-phys.net/10/10387/2010/, 2010.

Lee, A. K. Y., Willis, M. D., Healy, R. M., Onasch, T. B., and Abbatt, J. P. D.: Mixing state of carbonaceous aerosol in an urban environment: Single particle characterization using a soot particle aerosol mass spectrometer (SP-AMS), Atmospheric Chemistry and Physics, 15, 1823–1841, 2015.

Moosmller, H., Chakrabarty, R., and Arnott, W.: Aerosol light absorption and its measurement: A review, Journal of Quantitative Spectroscopy and Radiative Transfer, 110, 844 – 878, doi:http://dx.doi.org/10.1016/j.jqsrt.2009.02.035, URL

Response to Anonymous Referee # 2

The authors would like to thank Referee #2 for their comments on this manuscript, which have helped to improve the clarity of the paper. Our responses to specific comments and the corresponding changes to the manuscript are detailed below.

1. I like the style of this paper which is short and straightforward. But sometimes it is also inconvenient to always try to find things in supplement. Maybe the author can consider moving some important contents back to the main text.
Authors' response: Sections 2, 3, 4 and 7 of the Supplement have been added to the main paper, and Figures 1, 2 and 3 have been modified to include data from both the roadside and non-roadside sites. The discussion and figure relating to particle coating thickness estimation have also been added to the main text of the paper.

2. Fig. 5: It seems the SSA derived with PASS-3 measurement is with very large uncertainty.
Authors' response: We acknowledge that the measurements of SSA at 405 nm have a large amount of scatter, especially for the HOA-rich plume example shown in the paper (part (b) of the relevant figure). Uncertainty in the SSA measurement is impacted by uncertainty in both the absorption and scattering measurements. In particular, the SSA measurement is associated with a larger degree of scatter when the black carbon (and total aerosol) loading is low. This relatively large degree of scatter will arise when the black carbon loading is low and the instrument is approaching its detection limit. Since the SSA measurements are used as a qualitative illustration only, we do not believe that this uncertainty impacts any of the conclusions made in this work.

3. In the box model simulation a constant mixing height was assumed. There are studies based on PartMC-MOSAIC simulation suggest the diurnal evolution of mixing layer plays a very important role in the variation of aerosol mixing state (e.g. Liu et al., 2011). I am wondering if you will have largely different result if the variation of mixing layer is switched on.
Authors' response: We thank the reviewer for raising this point. We changed the text in the paper (i.e., text that was previously in Section 7 of the Supplement, and has been moved to the main paper) as follows: "The initial gas phase concentrations are the same as in Zaveri et al. (2010). In contrast to Zaveri et al. (2010), we prescribe a constant mixing height (400 m), relative humidity (70%) and temperature (298.15 K) to simplify the interpretation of the results. Since the entrainment of background aerosol can modify the aerosol mixing state substantially (Liu et al., 2011), we include constant dilution with the background at a rate of 1.5×10^{-5} s^{-1}. The background aerosol is non-absorbing and consists of ammonium sulfate mixed with biogenic secondary organic aerosol. This dilution rate corresponds to about 75% of the aerosol being replaced in a 24 h period, comparable to a diurnal mixing height increase of 500 m to 2000 m (e.g., Liu et al., 2011), although imposed uniformly over the day for simplicity."

4. Fig. 6: Are the calculated aerosol optical properties at dry state or ambient state (70% RH in your model)? I think it would be more interesting to see the results for ambient condition.

720 **Authors' response:** The aerosol optical properties are calculated for ambient conditions, i.e. we include the water content of the aerosol. To make this clear, we now address this explicitly in the Methods section as follows: "We calculate the optical properties for ambient conditions (including aerosol water content) at a wavelength of 550 nm and the critical supersaturations of each particle in a post-processing step according to Zaveri et al. (2010)."

5. P33559 L18-20: Overestimations in absorption efficiency would result in underestimates of SSA.

Authors' response: This error in wording has been corrected. The sentence has been revised to: "Previous work has clearly demonstrated that calculations of aerosol optical properties depend upon assumptions about particle mixing state, with assumptions of uniform internal mixing producing overestimates of absorption efficiency and underestimates of single scattering albedo."

6. P33560 L7: please define "rBC" here

Authors' response: Done. This sentence has been revised to: "...to assess the mixing state of refractory black carbon (rBC) containing particles derived from vehicle emissions."

7. P33561 L10: were used

Authors' response: Done.

8. P33566 L3: Fig. 4e and f

Authors' response: This error has been corrected in the revised manuscript.

9. P33582 L1: measurement-constrained

Authors' response: This error has been corrected.

10. Figures: both m^{-3} and $/cm^3$ are used in axis label. Please use the same style throughout the paper.

Authors' response: This inconsistency has been fixed, and cm^{-3} or m^{-3} is used in all figures.

References

Liu, P. F., Zhao, C. S., Göbel, T., Hallbauer, E., Nowak, A., Ran, L., Xu, W. Y., Deng, Z. Z., Ma, N., Mildenberger, K., Henning, S., Stratmann, F., and Wiedensohler, A.: Hygroscopic properties of aerosol particles at high relative humidity and their diurnal variations in the North China Plain, Atmo-

Response to Anonymous Referee # 3

Specific comments

We thank Referee #3 for their comments on this manuscript, which have helped us to more clearly communicate some of the complexities in this work. One issue which was brought up by all reviewers is the need to incorporate more details and discussion from the Supplement into the main paper. As a result, sections 2, 3, 4 and 7 of the Supplement have been moved into the main text. Our responses to specific comments and the corresponding changes to the manuscript are detailed below.

1. Page 33557 Line 10: define "HOA" in the abstract.
Authors' response: Done.

2. Page 33562, Line 5-7: Please be specific about "these calculations."
Authors' response: This sentence has been revised to "...that can impact the calculation of rBC mass fraction in rBC-containing particles."

3. Page 33563 Line 19: define "HOA" as this is the first time this term appears in the main text. Also I suggest that the authors briefly mention the speciation of the organics in Section 2.1 (e.g., in page 33561, line 14).
Authors' response: Hydrocarbon-like organic aerosol is now defined at the beginning of the results and discussion section in the revised manuscript. A sentence has been added to section 2.1 (page 33561, line 14) briefly describing the use of positive matrix factorisation to separate HOA, oxygenated organic aerosol (OOA), and biomass burning organic aerosol (BBOA), which is further described in the results and discussion.

4. Page 33564, Line 13: Are the BC particles in rBC-rich particles coated only with HOA-material? This statement sounded so but Figure 3 shows that there certainly are other types of coating materials such as nitrate and sulfate aerosols, which are often neglected in the discussion. For example, in Section 3.3, the effect of other (inorganic) coating materials on the modelled bulk particle hygroscopicity should also be discussed.
Authors' response: We acknowledge that this is a potentially confusing point, and we have made an effort to clarify these details related to mixing state in the main paper. The important point is that rBC-rich and HOA-rich particle classes from both studies are identified as those related to fresh emissions, and their average mass spectra from the cluster analysis do not contain detectable inorganic species (i.e., sulfate and nitrate). The sulfate and nitrate visible in the size distributions in Figure 3 are associated with more aged particle classes, which are not the focus of this work. In addition, sulfate and nitrate are correlated with OOA and BBOA factors from positive matrix factorisation, meaning that these species are associated with more aged and transported aerosol observed at the sampling sites. Therefore, when particles are emitted into the box model we consider that they contain rBC and HOA in varying amounts. The particles are aged in the model and become

mixed with inorganic species, influencing their hygroscopicity, but the different types of particles emitted into the model are aged in similar ways with respect to the condensation of inorganic species and therefore no differences in hygroscopicity are observed after 24 hours. The following sentence has been added to the main text of the paper in Section 3.2 to make this clearer:

"Positive matrix factorization (PMF) (Zhang et al., 2011; Ulbrich et al., 2009) indicates three major sources of rBC and organic aerosol in the roadside environment: transported biomass burning (BBOA), regional background (OOA), and traffic emissions comprised of two PMF factors (HOA-rich and rBC-rich factors, Figure 5c-f). Inorganic species evident in the bulk aerosol size distributions (Figure 3a and b) are largely associated with OOA and BBOA factors, while the traffic-related factors contain the majority of rBC and HOA. "

5. Page 33565, Line 11: It is stated that mf_{rBC} in HOA-rich factors is 0.16. I am a bit confused since in Page 33563 Line 26 the authors stated that the average mf_{rBC} in HOA-rich particles are 0.03 and 0.05 during the non-roadside and roadside studies. How are these numbers related?

Authors' response: The reviewer is correct that there is a difference in the mf_{rBC} between HOA-rich particle classes from single particle data, and the HOA-rich PMF factor derived from ensemble data. The likely cause of this discrepancy is related to the probability that we observe detectable rBC signals in a single particle. Since the sensitivity of the SP-AMS to rBC is relatively low (i.e., the sensitivity relative to ammonium nitrate is 0.2 ± 0.05) it is possible that on a per-particle basis we do not observe detectable rBC signal, or observe very few rBC ions per particle, and therefore may underestimate the mf_{rBC}. In the ensemble data, we are able to average signals for longer times, thus increasing our probability of observing detectable rBC signal and increasing mf_{rBC}. In support of this hypothesis, a substantial fraction of single particles in the HOA-rich class from the roadside study have mf_{rBC} near zero. But, since we detect some signal associated with these particles, we know that they must have contained some amount of rBC so that vaporization could occur. This bias in mf_{rBC} may also be due to incomplete evaporation of rBC-containing particles in the edges of the laser.

To clarify these differences and also to qualify our conclusion based on this potential measurement bias the following has been added to Section 3.2: "Differences in mf_{rBC} between single particle and ensemble measurements, especially for HOA-rich particles that contain a small amount of rBC, may be due to the probability of rBC detection in a single particle so that single particle mf_{rBC} may be underestimated relative to ensemble mf_{rBC} (Lee et al., 2015). "

6. Section 3.3: It would be good to compare the modelled particle absorption with the in situ PASS-3 measurement, which was very briefly mentioned in the method section and should be expanded, to assess the potential bias resulted from assuming a core/shell morphology using Mie calculation. Were there any scattering measurements during any or both of the studies? If so, it would be good to compare the modelled SSA with the measurement.

Authors' response: Firstly, regarding the lack of detail about the PASS measure-

ments, a new section has been added to the Methods section as follows: "A photoacoustic soot spectrometer (PASS-3, Droplet Measurement Techniques, Boulder, CO) was used to measure aerosol absorption (b_{abs}) and scattering (b_{abs}) coefficients (Mm^{-1}) at 405 and 781 nm. A 532 nm laser is not installed in this particular unit. The PASS determines aerosol absorption (Mm^{-1}) in a cavity which acts as an acoustic resonator. The absorption of incoming radiation heats the particles, which in turn heat the surrounding air in the cavity (Arnott et al., 1999). The aerosol-laden air thus expands, resulting in a pressure disturbance. By modulating the laser power at the resonance frequency of the cavity, the pressure disturbance is amplified and the resulting acoustic wave is measured using a microphone. Light scattering at both wavelengths is concurrently measured using reciprocal nephelometry (Moosmller et al., 2009; Flowers et al., 2010; Chan et al., 2011). Signals were not corrected for truncation; however, it should be noted that total particulate loading is relatively low at this site and saturation was not observed in scattering signals. The instrument was calibrated using a propane soot generator (miniCAST, 6203A, Jing); since a 532 nm laser was not present in this unit an NO_2 calibration was not possible. PASS measurements of the bulk single scattering albedo at 405 nm (selected due to superior signal-to-noise ratio for scattering relative to the 781 nm channel) are used here only to illustrate differences in optical properties in vehicle plumes with varying composition."

Secondly, regarding a direct comparison between measured and modelled absorption and scattering from the PASS, we do not believe that a direct comparison is viable, and may not be informative of biases introduced by the core-shell assumption, for the following three reasons. First, the modelled SSA is for 550 nm, while only measurements at 405 and 781 nm were available. Second, we measure the bulk SSA with the PASS, while we model the SSA of only a subset of the total aerosol population (i.e., those particles that contain rBC, measured by the SP-AMS). A sentence has been added to the main text of the paper to clarify this important difference. Thirdly, a direct comparison of the absorption with total rBC measured by the SP-AMS may not be quantitatively useful since we are aware that the SP-AMS has a lower size limit, owing to the aerodynamic lens, that means we underestimate rBC mass by missing smaller particles (i.e., those below ∼80 nm in vacuum aerodynamic diameter). This is also evident from the sharp decrease in rBC signals at small size in the size-resolved mass spectra. However, it is important to note that total rBC from the SP-AMS is well correlated with b_{abs} from the PASS measurements (this is detailed in Healy et al. (2015)). As noted above, the PASS measurements of SSA are included only to illustrate that we observe differences in optical properties in vehicle plumes with varying composition.

References

Arnott, W. P., Moosmller, H., Rogers, C. F., Jin, T., and Bruch, R.: Photoacoustic spectrometer for measuring light absorption by aerosol: instrument description, Atmospheric Environment, 33, 2845

– 2852, doi:http://dx.doi.org/10.1016/S1352-2310(98)00361-6, URL http://www.sciencedirect.com/science/article/pii/S1352231098003616, 1999.

Chan, T. W., Brook, J. R., Smallwood, G. J., and Lu, G.: Time-resolved measurements of black carbon light absorption enhancement in urban and near-urban locations of southern Ontario, Canada, Atmospheric Chemistry and Physics, 11, 10 407–10 432, doi:10.5194/acp-11-10407-2011, URL http://www.atmos-chem-phys.net/11/10407/2011/, 2011.

Flowers, B. A., Dubey, M. K., Mazzoleni, C., Stone, E. A., Schauer, J. J., Kim, S.-W., and Yoon, S. C.: Optical-chemical-microphysical relationships and closure studies for mixed carbonaceous aerosols observed at Jeju Island; 3-laser photoacoustic spectrometer, particle sizing, and filter analysis, Atmospheric Chemistry and Physics, 10, 10 387–10 398, doi:10.5194/acp-10-10387-2010, URL http://www.atmos-chem-phys.net/10/10387/2010/, 2010.

Healy, R. M., Wang, J. M., Jeong, C.-H., Lee, A. K. Y., Willis, M. D., Jaroudi, E., Zimmerman, N., Hilker, N., Murphy, M., Eckhardt, S., Stohl, A., Abbatt, J. P. D., Wenger, J. C., and Evans, G. J.: Light-absorbing properties of ambient black carbon and brown carbon from fossil fuel and biomass burning sources, Journal of Geophysical Research: Atmospheres, 120, 6619–6633, doi:10.1002/2015JD023382, 2015.

Lee, A. K. Y., Willis, M. D., Healy, R. M., Onasch, T. B., and Abbatt, J. P. D.: Mixing state of carbonaceous aerosol in an urban environment: Single particle characterization using a soot particle aerosol mass spectrometer (SP-AMS), Atmospheric Chemistry and Physics, 15, 1823–1841, 2015.

Moosmller, H., Chakrabarty, R., and Arnott, W.: Aerosol light absorption and its measurement: A review, Journal of Quantitative Spectroscopy and Radiative Transfer, 110, 844 – 878, doi:http://dx.doi.org/10.1016/j.jqsrt.2009.02.035, URL http://www.sciencedirect.com/science/article/pii/S0022407309000879, light Scattering: Mie and More Commemorating 100 years of Mie's 1908 publication, 2009.

Ulbrich, I. M., Canagaratna, M. R., Zhang, Q., Worsnop, D. R., and Jimenez, J. L.: Interpretation of organic components from Positive Matrix Factorization of aerosol mass spectrometric data, Atmospheric Chemistry and Physics, 9, 2891–2918, 2009.

Zhang, Q., Jimenez, J. L., Canagaratna, M. R., Ulbrich, I. M., Ng, N., Worsnop, D., and Sun, Y.: Understanding atmospheric organic aerosols via factor analysis of aerosol mass spectrometry: A review, Anal. Bioanal. Chem., 401, 3045–3067, doi:10.1007/s00216-011-5355-y, 2011.

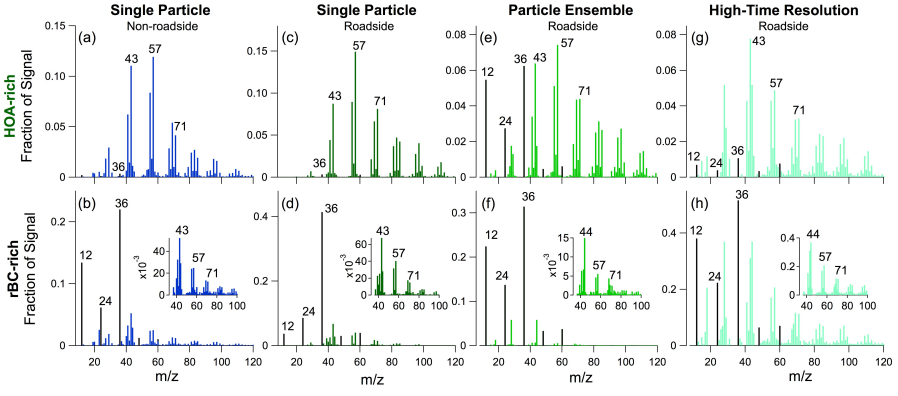

Figure 1. Unit mass resolution (UMR) spectra of HOA-rich **(a)** and rBC-rich **(b)** particle classes identified by *k*-means cluster analysis of single particle SP-AMS data acquired in the non-roadside environment.UMR spectra of HOA-rich **(c)** and rBC-rich **(d)** particle classes identified from single particle data in the roadside environment. High-resolution mass spectra of HOA-rich **(e)** and rBC-rich **(f)** PMF factors from ensemble SP-AMS data from the roadside study (i.e., for rBC-containing particles only). Examples of UMR spectra collected at high-time resolution during HOA-rich **(g)** and rBC-rich **(h)** plumes (corresponding time series are shown in Figure 6) during the roadside study. Insets in the lower panels illustrate the UMR spectrum of organic species (without CO_x^+ fragments) in the rBC-rich mass spectra. Black and colored sticks represent the fragments of rBC (C_x^+) and organic species($C_xH_y^+$,$C_xH_yO_w^+$), respectively.

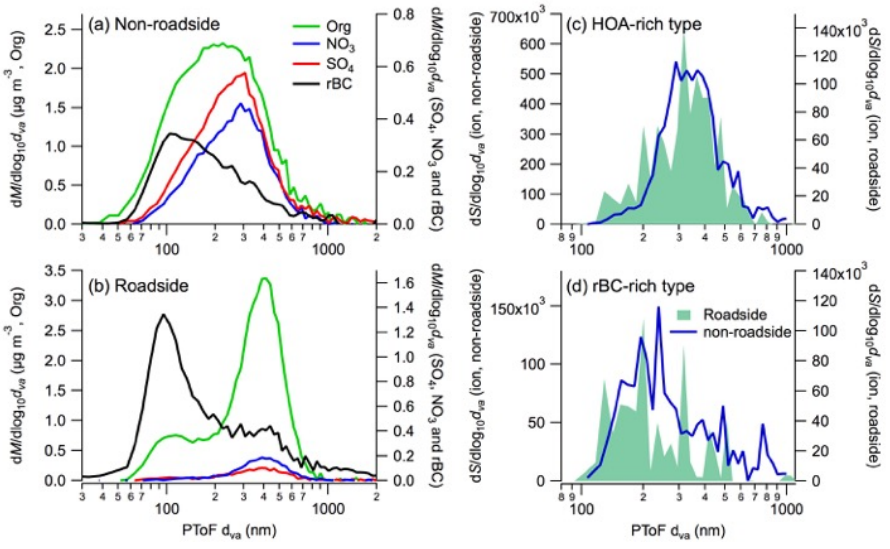

Figure 2. Particle size distributions from the non-roadside and roadside studies.**(a)** Mass-based ensemble size distribution of refractory black carbon (rBC, black), organic species (Org, green), sulphate (SO_4, red) and nitrate (NO_3, blue) for the non-roadside study.**(b)** Mass-based ensemble size distribution from the roadside study. **(c)** Ion-signal based single particle size distributions for HOA-rich particle classes from the roadside (filled green) and non-roadside (blue) studies.**(d)** Ion-signal based single particle size distributions for rBC-rich particle classes from the roadside (filled green) and non-roadside (blue) studies.The SP-AMS measured rBC-containing particles only during the roadside study, while both rBC-containing and non-rBC-containing particles were measured in the non-roadside study.

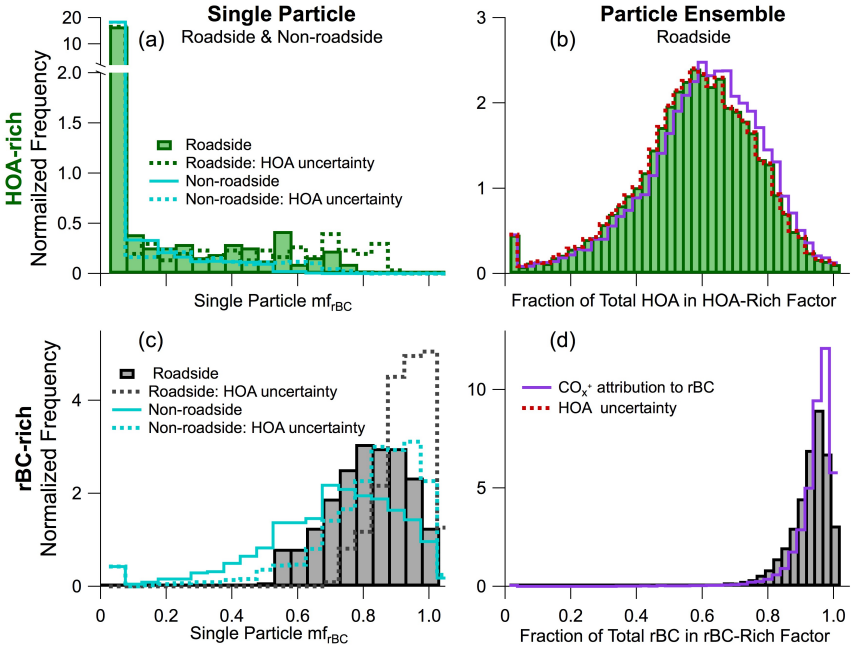

Figure 3. **(a)** & **(c)** The distribution of mf_{rBC} (presented as a normalized histogram) in the HOA-rich **(a)** and rBC-rich **(c)** particle classes in roadside (green and black) and non-roadside (blue) environments. Bars and solid lines represent mf_{rBC} calculated from rBC fragments (i.e. C_x^+), and dashed lines represent the impact of a 50 % decrease in HOA mass loading, to illustrate the impact of uncertainty in HOA quantification. **(b)** & **(d)** Normalized histograms of mf_{Org} in the HOA-rich factor **(b)** and mf_{rBC} in the rBC-rich factor **(d)**, i.e., frequency distribution showing the fraction of total rBC (HOA) contributed by the rBC-rich (HOA-rch) factor. Bars represent mf_{rBC} calculated by rBC fragments (i.e. C_x^+), whereas purple dashed lines represent the mf_{rBC} calculated including both CO_x^+ and C_x^+ fragments, yielding similar results (see Supplement Sect. 1). Red dashed lines represent the impact of a 50 % decrease in HOA mass loading, to illustrate the impact of uncertainty in HOA quantification.

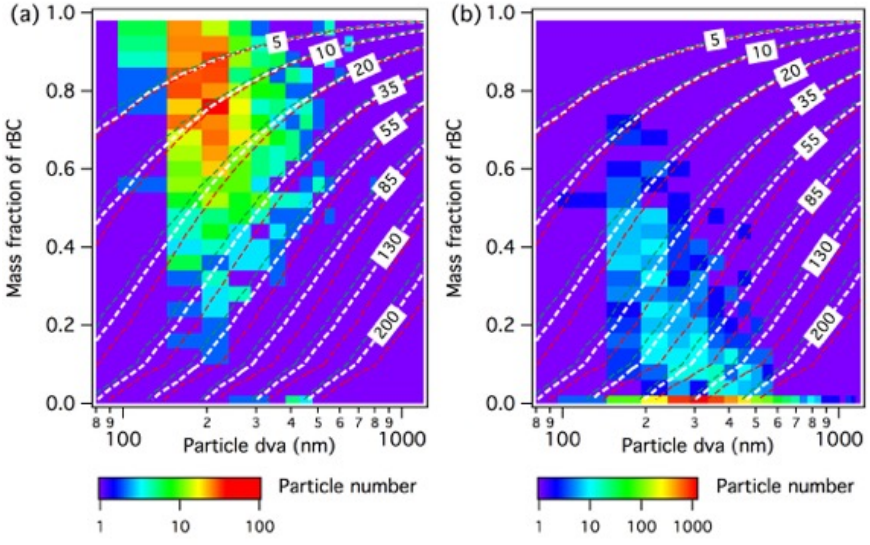

Figure 4. Two-dimensional histograms (mf_{rBC} vs. particle aerodynamic diameter) of rBC-rich **(a)** and HOA-rich **(b)** particle classes. The color scale represents the number of particles in each particle class. The dashed lines represent the physical thickness (nm) of organic coating on rBC-containing particles determined by modelling the particles as a core-shell structure. Note that the d_{va} of model outputs are calculated by the physical diameter (d_p) and the density (ρ_p) of particles (i.e., $d_{va} = d_p \cdot \rho_p$ where ρ_p is the linear combination of mass-weighted HOA and rBC density). To examine the potential effect of fractal structure of ambient rBC particles on predicted coating thickness, the effective density of rBC was varied (green: 0.3 g cm^{-3}, white: 0.8 g cm^{-3}, and red: 1.3 g cm^{-3}).

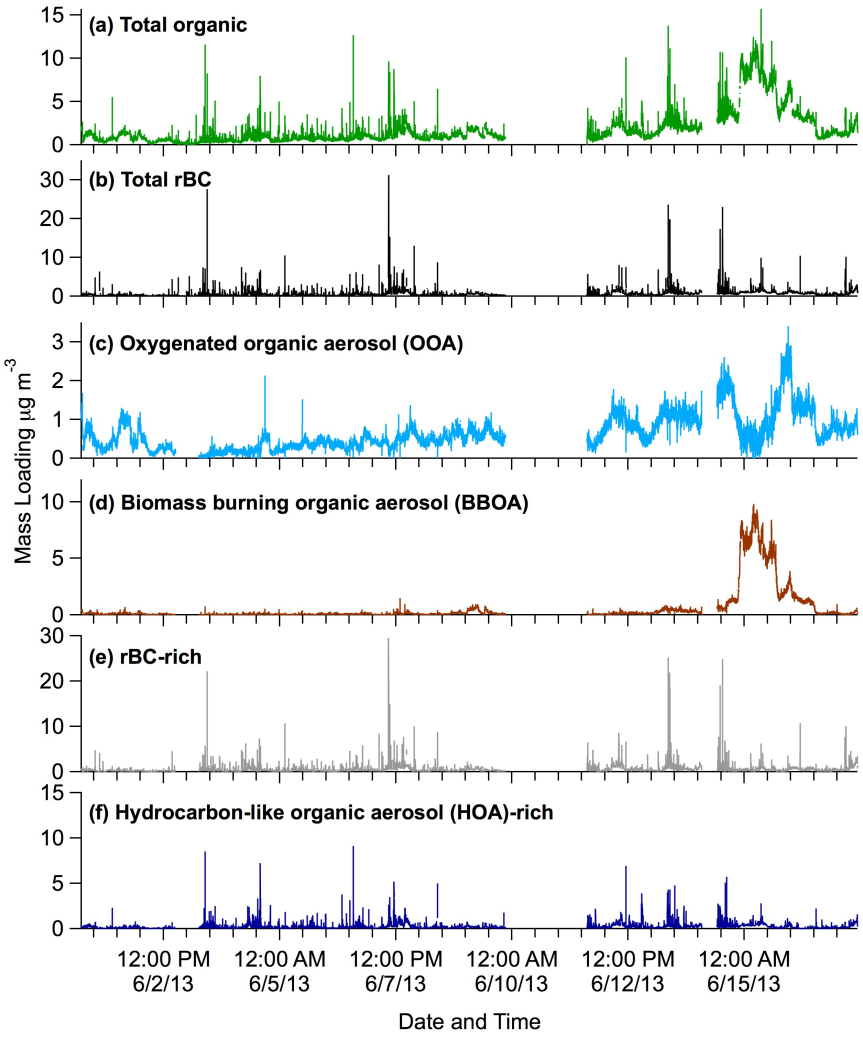

Figure 5. Time series of **(a)** ensemble organic aerosol and **(b)** refractory black carbon mass loadings during the roadside study. Positive matrix factorization (PMF) results for ensemble data **(c)** to **(f)**: **(c)** regionally sourced rBC mixed with oxygenated organic aerosol, **(d)** biomass-burning organic aerosol mixed with rBC, and traffic-related rBC in an rBC-rich and HOA-rich factor **(e)** and **(f)**. Mass spectra of all PMF factors are shown in Fig. S1 in the Supplement.

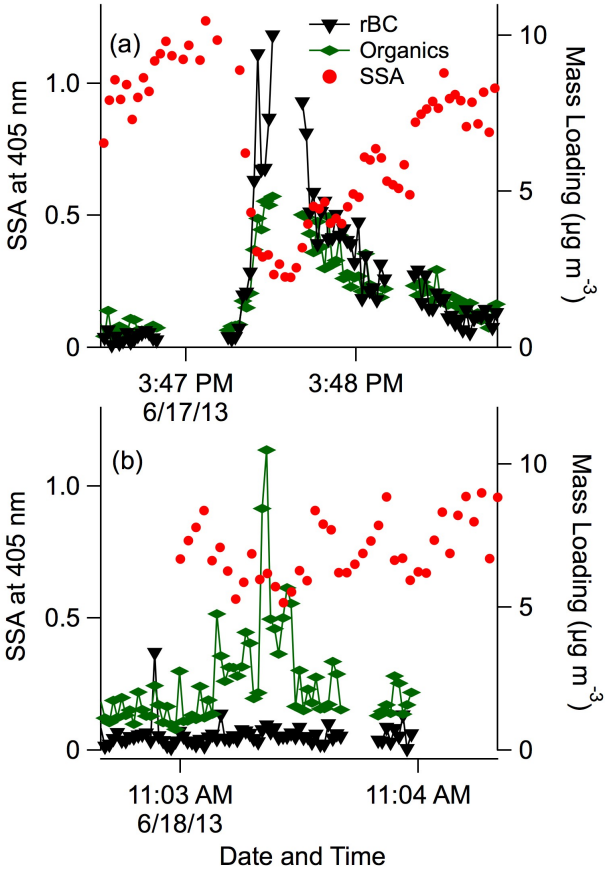

Figure 6. Examples of rBC-dominated **(a)** and organic-dominated **(b)** plumes observed using the SP-AMS with high-time resolution (1 Hz) sampling, with measurements of single scattering albedo (SSA) at 405 nm from a photoacoustic soot spectrometer (PASS-3). Gaps in SP-AMS data correspond to periods used for the subtraction of gas-phase contributions from particle signals. Mass spectra shown in Figure 1**(g)** and **(h)** correspond to plumes in **(b)** and **(a)**, respectively.

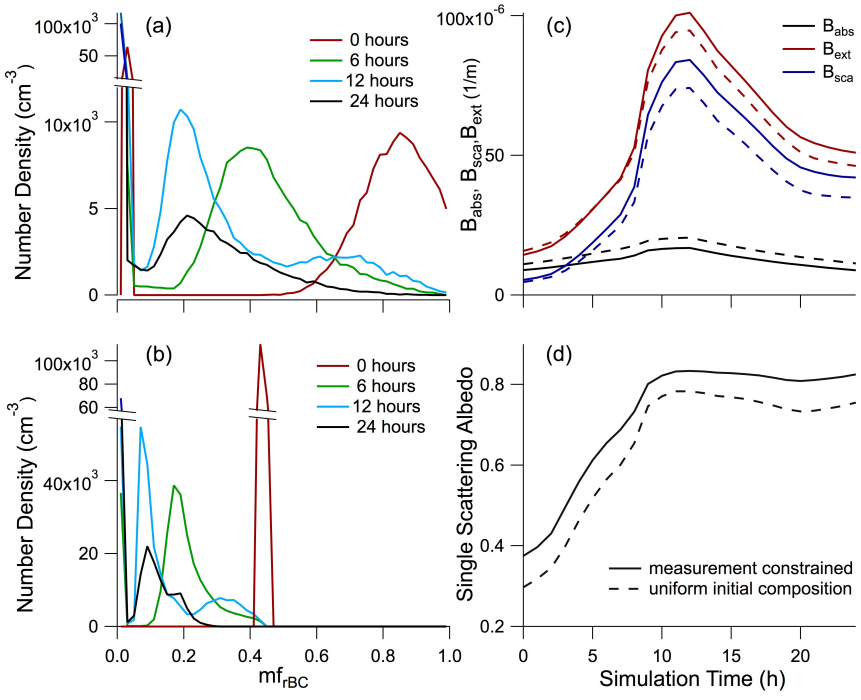

Figure 7. Evolution of dry mf_{rBC} for the measurement-constrained **(a)** and uniform initial **(b)** mixing state cases. See Methods and Supplement Sect. 3 for a description of the model input parameters. Evolution of volume absorption (B_{abs}), scattering (B_{scat}) and extinction (B_{ext}) coefficients at 550 nm **(c)**, and single scattering albedo (SSA) at 550 nm over the 24h simulation period **(d)** for measurement constrained (solid lines) and uniform initial mixing state (dashed lines) cases.